

A Survey of Generative AI for *de novo* Drug Design: New Frontiers in Molecule and Protein Generation

Xiangru Tang^{1*}, Howard Dai^{1*}, Elizabeth Knight^{1*}, Fang Wu², Yunyang Li¹, Tianxiao Li¹ and Mark Gerstein¹

¹Yale University, New Haven, CT, USA and ²Tsinghua University, China

*Contributed equally to this work.

Abstract

Artificial intelligence (AI)-driven methods can vastly improve the historically costly drug design process, with various generative models already in widespread use. Generative models for *de novo* drug design, in particular, focus on the creation of novel biological compounds entirely from scratch, representing a promising future direction. Rapid development in the field, combined with the inherent complexity of the drug design process, creates a difficult landscape for new researchers to enter. In this survey, we organize *de novo* drug design into two overarching themes: small molecule and protein generation. Within each theme, we identify a variety of subtasks and applications, highlighting important datasets, benchmarks, and model architectures and comparing the performance of top models. We take a broad approach to AI-driven drug design, allowing for both micro-level comparisons of various methods within each subtask and macro-level observations across different fields. We discuss parallel challenges and approaches between the two applications and highlight future directions for AI-driven *de novo* drug design as a whole. An organized repository of all covered sources is available at <https://github.com/gersteinlab/GenAI4Drug>.

Key words: Generative Model, Drug Design, Molecule Generation, Protein Generation

Introduction

During the drug design process, ligands must be created, selected, and tested for their interactions and chemical effects conditioned on specific targets [1]. These ligands range from small molecules with tens of atoms to large proteins such as monoclonal antibodies [2, 3]. While methods exist to optimize the selection and testing of probable molecules, traditional discovery methods across all fields are computationally expensive [4]. Recent artificial intelligence (AI) models have demonstrated competitive performance [5, 6, 7] in improving various tasks in the drug design process. Methods such as machine learning (ML)-driven quantitative structure-activity relationship (QSAR) approaches [8, 9] have significantly improved virtual screening (VS) in molecule design [10, 11], while ML-assisted directed evolution techniques for protein engineering [12, 13] have proven to be reliable and widely used tools. However, an emerging and even more powerful task for ML is the generation of entirely new biological compounds in *de novo* drug design [14, 15, 16].

In contrast to applications in VS and directed evolution, which seek to expedite and optimize tasks within an existing framework, *de novo* drug design focuses on generating entirely new biological entities not found in nature [14]. While other ML-driven methods search within existing chemical libraries for drug-like candidates, thereby facing inherent constraints, *de novo* design circumvents this limitation by exploring unknown chemical space and generating drug-like candidates from scratch [24, 25, 26].

In this paper, we explore the impacts and developments of ML-driven *de novo* drug design in two primary areas of research: **molecule** and **protein** generation. Within protein generation, we explore antibody generation in particular, given

its high research activity and relevance. Although the types of pharmaceuticals and the associated chemical nuances differ across fields, the overarching goal of exploring chemical space through *de novo* design remains constant. All three fields are rapidly growing industries with traditionally high research and development costs [27, 28, 29], and current improvements are driven by active developments in ML-based *de novo* methods.

Molecule design specifically refers to the development of novel molecular compounds, often with the aim of small-molecule drug design. The generated molecules must satisfy a complex and often abstract array of chemical constraints that determine both their validity and “drug-likeness” [30, 31]. This, combined with the vast space of potential drug-like compounds (up to 10^{23} - 10^{60} [32]), renders traditional small-drug design time-consuming and expensive. Using traditional methods, preclinical trials can cost hundreds of millions of dollars [33] and take between 3 and 6 years [4]. In recent years, AI-driven methods have gained traction in drug design. AI-focused biotechnology companies have initiated over 150 small-molecule drugs in the discovery phase and 15 in clinical trials, with the usage of this AI-fueled process expanding by almost 40% each year [34].

An equally promising field, *protein design*, refers to the artificial generation or modification of proteins (protein engineering) for various biological uses. Native proteins have adapted and evolved over millions of years, so the rapid progression of human society in recent years poses challenges for naturally occurring proteins [35]. Protein design has an even more versatile range of applications, finding utility in immune signaling, targeted therapeutics, and various other fields. When executed efficiently, protein design has the potential to transform synthetic biology [36, 37, 28]. Like molecule generation, proteins must adhere to abstract biological

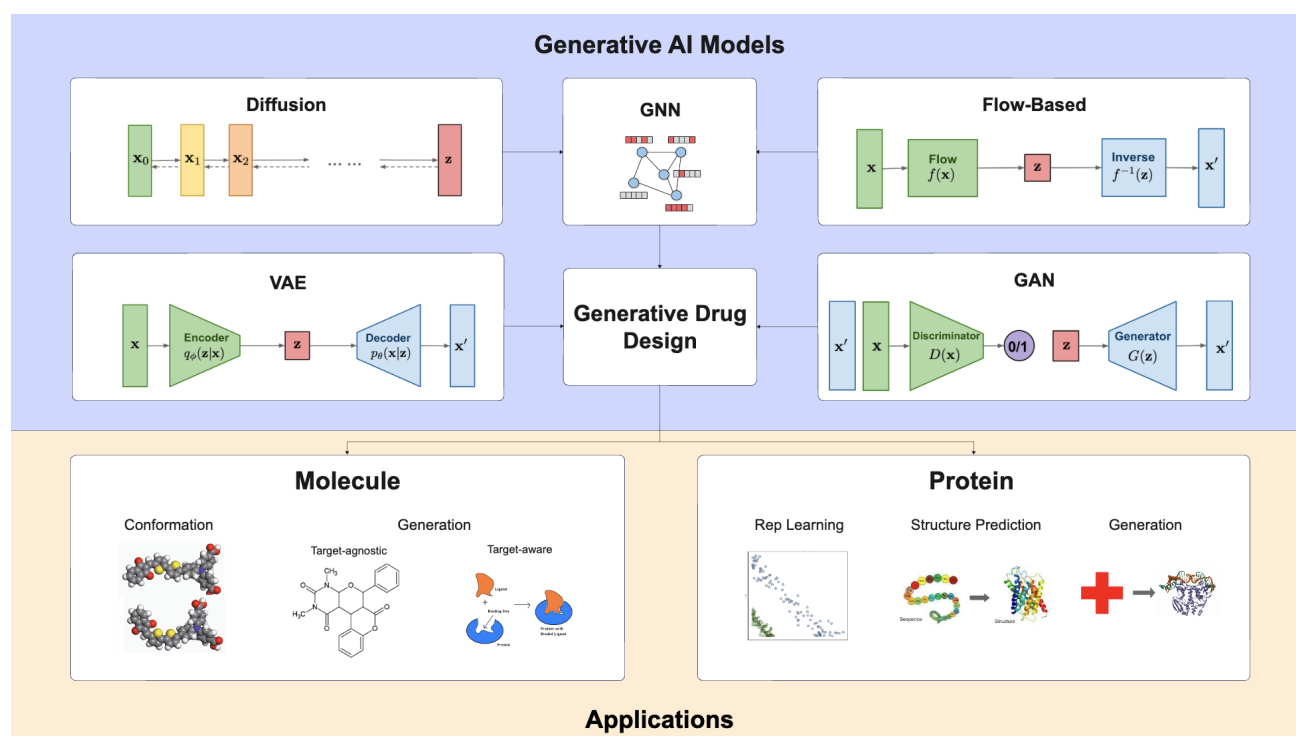


Fig. 1. An overview of the topics covered in this survey. In particular, we explore the intersection between generative AI model architectures and real-world applications, organized into two main categories: small molecule and protein generation tasks. Note that diffusion and flow-based models are often paired with GNNs for processing 2D/3D-based input, while VAEs and GANs are typically used for 1D input. Images used from [17, 18, 19, 20, 21, 22, 23].

constraints, yet the inherently more complex structure of a protein presents a nuanced generative objective, requiring a more direct application of chemical knowledge in the process [38, 39, 40]. Traditional methods such as directed evolution are confined to specific evolutionary trajectories for existing proteins, thus limiting their scope. The *de novo* generation of proteins would add an entirely new dimension for researchers to explore [41, 37, 42].

Structurally, we aim to provide an organized introduction to the two fields mentioned above. We begin with a technical overview of relevant deep learning architectures employed in both small molecule and protein design. We then explore their applications in molecule and protein design, dividing our analysis into a variety of subfields highlighted in Figure 1. For each subfield, we provide (1) a general background/task definition, (2) common datasets used for training and testing, (3) common evaluation metrics, (4) an overview of past and current ML approaches, and (5) a comparative analysis of the performance of state-of-the-art (SOTA) models. A detailed overview of this structure is shown in Figure 2. Finally, we integrate concepts within each subfield into a broad analysis of *de novo* drug design as a whole, providing a comprehensive summary of the field in terms of current trends, top-performing models, and future directions. Our overall objective is to provide a systematic overview of ML in drug design, capturing recent advancements in this rapidly evolving area of research.

Related Surveys

Several survey papers delve into specific aspects of generative AI in drug design, with some focusing on molecule generation [24, 43, 44], protein generation [35, 36], or antibody generation [45, 46, 47, 48]. Other survey papers are organized based on

model architecture rather than application, with recent papers by Zhang et al. [49] and Guo et al. [50] reviewing diffusion models in particular. While each of the above surveys provides an in-depth analysis of a specific application or type of model, the level of specialization may limit their scope. Our approach is a macro-level analysis of small molecule and protein generation, tailored for those seeking a high-level introduction to the emerging field of generative AI in chemical innovation. This broad perspective enables us to highlight relationships across fields, such as parallel shifts in methods of input representation, the common emergence of architectures like equivariant graph neural networks (EGNNs), and similar challenges faced in both molecule and protein design.

Preliminary: Generative AI Models

Generative AI uses various statistical modeling, iterative training, and random sampling to generate new data samples resembling the input data. Historically, prominent approaches include generative adversarial networks (GANs) [51], variational autoencoders (VAEs) [52], and flow-based models [53]. More recently, diffusion models [54] have emerged as promising alternatives. In our survey, we begin by providing a concise mathematical and computational overview of these architectures.

Variational Autoencoders

A VAE [52] is a type of generative model that extends upon the typical encoder-decoder framework by representing each latent attribute using a distribution rather than a single value. This approach creates a more dynamic representation for the underlying properties of the training data and enables the sampling of new data points from scratch. Formally, we can

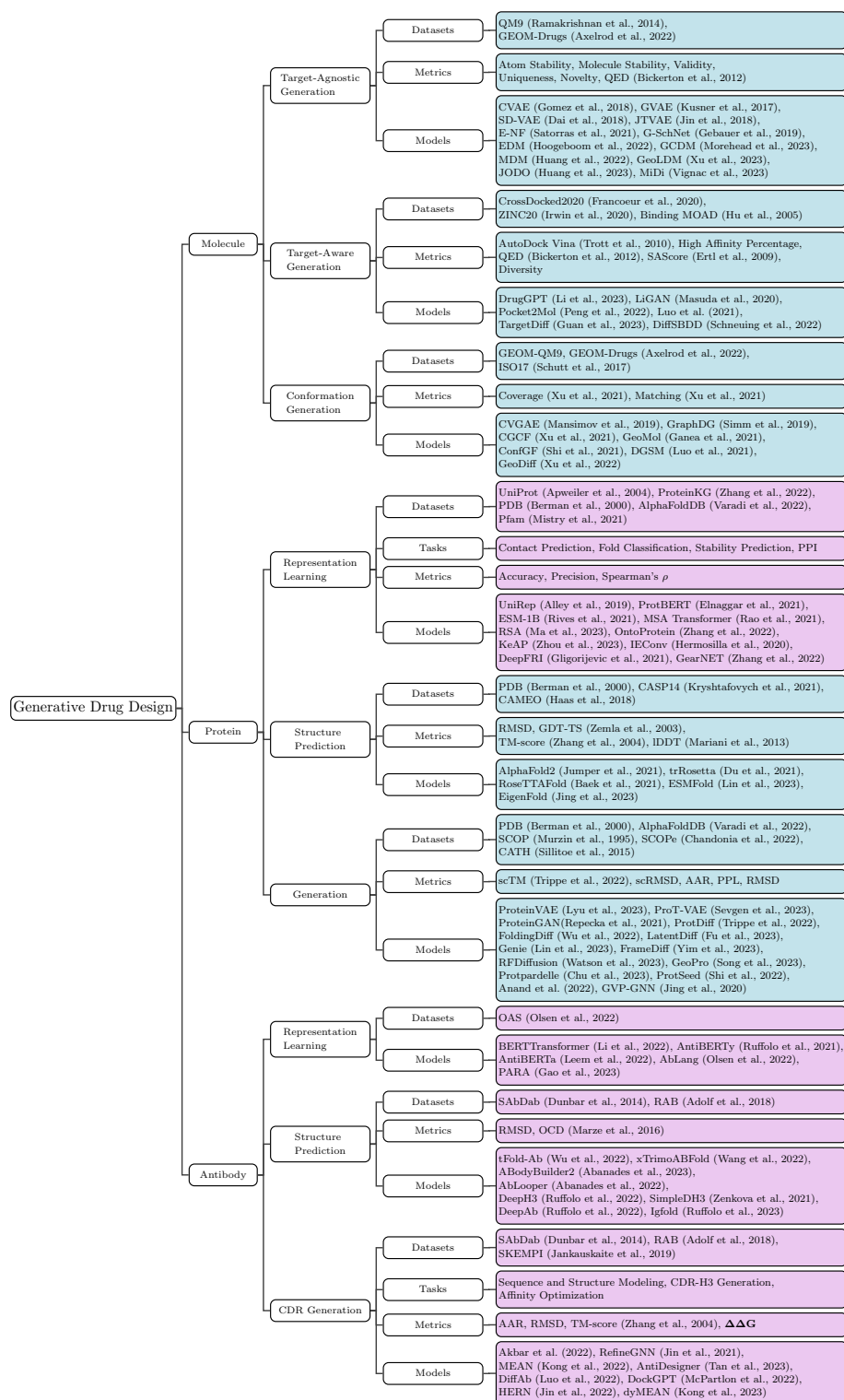


Fig. 2. A structured layout for all terms and papers covered in our survey, including datasets, models, and metrics for each task. Sections contained in the main text are highlighted in blue, while sections expanded upon in the appendix are highlighted in purple.

express the encoder as:

$$q_\phi(z|x) = \mathcal{N}(z; \mu_\phi(x), \sigma_\phi^2(x)I)$$

Intuitively, each x will be mapped to some mean $\mu_\phi(x)$ and variance $\sigma_\phi^2(x)$, which describe a corresponding normal distribution. We express the decoder as $p_\theta(x|z)$, where z is a randomly sampled point from the latent distribution $\mathcal{N}(\mu_\phi(x), \sigma_\phi^2(x)I)$ and is mapped into a point x in the decoding process.

VAE loss is computed using two balancing ideas: reconstruction loss and Kullback–Leibler (KL) divergence loss. Reconstruction loss measures the difference between the ground truth and the reconstructed decoder output, often expressed using cross-entropy loss:

$$\mathcal{L}_{\text{recon}} = -1 * \int q_\phi(z|x) \log p_\theta(x|z) dz$$

KL divergence measures the difference between two probability distributions [55]. For VAEs, KL divergence is computed between the encoded distribution and the standard normal distribution. This can be seen as “regularization,” as it encourages the encoder to map elements to a more central region with overlapping distributions, thus improving continuity across the latent space. Formally, the KL loss can be expressed as follows, with k representing the k th dimension in the latent space:

$$\mathcal{L}_{\text{KL}} = D_{\text{KL}}(q_\phi(z|x) || \mathcal{N}(0, I)) = -\frac{1}{2} \sum_k \left(1 + \log(\sigma_k^2) - \mu_k^2 - \sigma_k^2 \right)$$

Then, the overall loss function can be expressed as follows, where β can be adjusted to balance the reconstruction loss and KL loss:

$$\mathcal{L} = \mathcal{L}_{\text{recon}} + \beta \mathcal{L}_{\text{KL}}$$

Generative Adversarial Networks

GANs [51] utilize “competing” neural networks for mutual improvement. The two neural networks — the generator and the discriminator — compete in a zero-sum game. The generator (G) creates instances (e.g., chemical structures of potential drugs) from random noise (z) sampled from a prior distribution $p_z(z)$ to mimic the training samples, while the discriminator (D) aims to distinguish between the synthetic data and the training samples.

The learning process involves the optimization of the following loss function:

$$\min_G \max_D \mathbb{E}_x [\log D(x; \theta_d)] + \mathbb{E}_{z \sim p(z)} [\log(1 - D(G(z; \theta_g); \theta_d))]$$

Here, $\mathbb{E}_x [\log D(x; \theta_d)]$ represents the likelihood applied by the discriminator to a correct sample, while $\mathbb{E}_{z \sim p(z)} [\log(1 - D(G(z; \theta_g); \theta_d))]$ represents the negative likelihood applied by the discriminator to an incorrect sample. This function returns a higher value when the discriminator accurately categorizes samples; thus, the discriminator aims to maximize this function, while the generator aims to minimize it.

Flow-Based Models

Flow-based generative models [53] generate data according to a target distribution $x \sim p(x)$ by applying a chain of transformations to a simple latent distribution, often Gaussian,

denoted $z_0 \sim p_0(z_0)$. This transformation applies an invertible function $f : z_0 \mapsto x$, such that:

$$x = f(z; \theta) \Rightarrow z = f^{-1}(x; \theta)$$

where the trained model learns parameters θ . Since f is invertible and thus the learned map is bijective, z has the same dimensionality as x . Often, f is a composite function where $f(x) = f_K \circ f_{K-1} \circ \dots \circ f_1(x)$; this allows for more complex probability distributions to be modeled. Because each function is invertible, the posterior can be easily computed — the log-likelihood of a single point x can be written in terms of its latent variable z :

$$\log p(x) = \log p_0(z) + \log \left| \det \frac{\partial f}{\partial z} \right|$$

This function is used to train parameters θ to maximize the probability of observing the data. Various models build upon this premise to represent complex data distributions and capture relationships within sequential data.

Diffusion Models

Diffusion models [54] perform a fixed learning procedure, gradually adding Gaussian noise to data over a series of time steps. We define two stages of the model: the noise-adding (forward) and the noise-removing (reverse) process.

In the forward process, each step x_{t+1} can be represented as a Markov chain and is comprised of x_{t-1} and a small amount of Gaussian noise. We represent this mathematically as follows:

$$x_{t+1} = \sqrt{1 - \beta_t} x_t + \sqrt{\beta_t} \epsilon, \quad \epsilon \sim \mathcal{N}(0, I)$$

Here, x_t is the data at time t , and β_t denotes the noise schedule. The variance β_t decreases in the forward process so that after many steps, we have $p(x_t|x_0) \approx \mathcal{N}(0, 1)$.

In the reverse process, our aim is to reconstruct the data from the noise. In this process, a denoising function is learned, often modeled by a neural network:

$$x_{t-1} = f_\theta(x_t, t) + \sqrt{\beta_t} \epsilon, \quad \epsilon \sim \mathcal{N}(0, I)$$

where $f_\theta(x_t, t)$ is the denoising function parameterized by θ .

To train a diffusion model, we approximate the added noise at each step; the loss function minimizes the difference between the true noise and the model-predicted noise:

$$L_t = \mathbb{E}_{t \sim [1, T], x_0, \epsilon_t} [\|\epsilon_t - \epsilon_\theta(x_t, t)\|^2]$$

Here, $t \sim U\{1, T\}$ means that the time step t is drawn uniformly at random from the set $\{1, 2, \dots, T\}$, and $\epsilon_\theta(x_t, t)$ represents the noise predicted by the model parameterized by θ . T represents the last time step of the model. Once the neural network has been trained, we can sample from the noise distribution and iterate through the reverse process to generate new data.

Diffusion models can be further categorized into three subtypes. *Denoising diffusion probabilistic models (DDPMs)* [56] focus on an iterative denoising process, where the reverse function is learned by a neural network that gradually removes the added noise. *Score-based generative models (SGMs)* [57] instead estimate the gradient (score function) of the data distribution at each timestep, using it to subtract the error

from the current representation. While the objective is framed differently, Ho et al. [56] demonstrate that the SGM is equivalent to a DDPM during training, albeit under a different parameterization. Finally, *stochastic differential equation (SDE)-based models* [58] extend SGMs and DDPMs by learning continuous-time diffusion processes using Ito’s calculus [59].

While the mathematical framework for the diffusion process is generally based on continuous data, adaptations made by Austin et al. [60] allow for smoother implementation with discrete data forms like molecular graphs.

Graph Neural Networks

While graph neural networks (GNNs) [61] are not inherently generative models on their own, they represent important components of larger generative methods. GNNs are especially important for processing graph-structured data. In the context of proteins, nodes and edges represent amino acids and spatial or sequential proximity, respectively. Once data have been transformed into a graph $G = (V, E)$ with nodes V and edges E , the GNN learns to map nodes to embeddings through message passing and aggregation. For each pair of nodes v_i, v_j , a GNN learns a “message” \mathbf{m}_{ij} based on existing features $\mathbf{h}_i^l, \mathbf{h}_j^l$ and coordinates $\mathbf{x}_i^l, \mathbf{x}_j^l$ at layer l (a_{ij} denotes the (i, j) entry in adjacency matrix A):

$$\mathbf{m}_{ij} = \phi_e(\mathbf{h}_i^l, \mathbf{h}_j^l, \mathbf{x}_i^l, \mathbf{x}_j^l, a_{ij})$$

Then, the message received by any node v_i is an aggregation of the messages from its neighbors:

$$\mathbf{m}_i = \sum_{j \in \mathcal{N}(i)} \mathbf{m}_{ij}$$

Finally, another network learns to combine old embeddings and positions with messages to create new embeddings and positions at layer $l + 1$:

$$\mathbf{h}_i^{l+1}, \mathbf{x}_i^{l+1} = \phi_h(\mathbf{h}_i^l, \mathbf{x}_i^l, \mathbf{m}_i)$$

Note that positions \mathbf{x} and features \mathbf{h} are often concatenated and denoted as a singular feature vector \mathbf{h} , as they are treated equivalently in the general GNN case.

Equivariant Graph Neural Networks

For the generation of 3D structures, equivariance is a useful inductive bias to incorporate into deep learning models. In general, two 3D structures should be treated equally if they only differ under a series of rotations, reflections, and translations.

For some conditional distribution $p(y|x)$, it is equivariant to the action of rotations and reflections when $p(Ry) = Rp(y)$ (alternatively, $p(y|x) = p(Ry|Rx)$) for transformation R . A distribution is invariant if $p(Ry) = p(y)$. In most works, the transformations consist of the Euclidean E(3) group generated by rotations, translations, and reflections.

Satorras et al. [62] propose the EGNN, a simple adjustment to the traditional GNN framework to preserve equivariance. This is accomplished by defining separate point embeddings \mathbf{x}_i and feature embeddings \mathbf{h}_i for each node v_i , and considering relative positions for message passing:

$$\begin{aligned} \mathbf{m}_{ij} &= \phi_e(\mathbf{h}_i^l, \mathbf{h}_j^l, \|\mathbf{x}_i^l - \mathbf{x}_j^l\|, a_{ij}) \\ \mathbf{x}_i^{l+1} &= \mathbf{x}_i^l + C \sum_{j \neq i} (\mathbf{x}_i^l - \mathbf{x}_j^l) \phi_x(\mathbf{m}_{ij}) \end{aligned}$$

The final message aggregating and embedding update steps are equivalent to that of a GNN. Here, equivariance is preserved

because we only consider relative positions/distances $\mathbf{x}_i^l - \mathbf{x}_j^l$ in message passing. Therefore, rotating, translating, or reflecting all atoms will result in equivalent functions.

Other Models

While we cover the main generative methods used in these fields, a variety of other models also appear in specific applications and tasks in our paper, such as transformers, energy-based models (EBMs), BERT, and more [63, 64, 65, 66, 67, 68, 69]. Beyond eGNNs, a wide variety of other GNN variations exist, including message-passing neural networks (MPNNs) [70], graph convolutional networks (GCNs) [71], graph isomorphism networks (GINs) [72], and convolutional neural networks (CNNs) [73, 74, 75].

Applications

Molecule

Task Background

Molecule generation focuses on the creation of novel molecular compounds for drug design. These generated molecules are intended to be (1) valid, (2) stable, and (3) unique, with an overall goal of pharmaceutical applicability. “Pharmaceutical applicability” is a broad term for a molecule’s binding affinity to various biological targets. While the first three tasks may seem trivial, there are a variety of challenges with simply generating valid and stable molecules. Thus, the field of *target-agnostic* molecule generation is focused on generating valid sets of molecules without consideration for any biological target. *Target-aware* molecule generation (or ligand generation) focuses on the generation of molecules for specific protein structures and therefore focuses more on the pharmaceutical component. Finally, *3D conformation generation* involves generating various 3D conformations given 2D connectivity graphs.

For training and testing, molecule inputs can be formatted in a variety of ways, depending on the available information or desired output. Molecules can be expressed in 1D format through the simplified molecular-input line-entry system (SMILES), in 2D using connectivity graphs to represent bonds, or in 3D using point cloud embeddings on graph nodes [76].

Target-Agnostic Molecule Design

Overview

While the task of target-agnostic molecule design may seem simplistically open-ended, there are a vast array of chemical properties and rules that generated molecules must align with to be considered “valid” and “stable.” The determination of “validity” includes a complex combination of considerations, such as electromagnetic forces, energy levels, and geometric constraints, and a well-defined “formula” does not yet exist for predicting the feasibility of molecular compounds. This, combined with the vast space of potential drug-like compounds (up to $10^{23} - 10^{60}$), makes brute-force experimentation quite time-consuming [32]. Deep learning can assist in learning abstract features for existing valid compounds and efficiently generate new molecules with a higher likelihood of validity.

Datasets

To learn these abstract constraints, models must learn from large sets of existing valid, stable molecules. The following datasets are most commonly used for this task:

Model	Type of Model	Dataset	At Stb. (% , \uparrow)	Mol Stb. (% , \uparrow)	Valid (% , \uparrow)	Val/Uniq. (% , \uparrow)
G-SchNet [80]	SchNet	QM9	95.7 [81]	68.1 [81]	85.5 [81]	80.3 [81]
E-NF [82]	EGNN, Flow	QM9	85 [81]	4.9 [81]	40.2 [81]	39.4 [81]
EDM [81]	EGNN, Diffusion	QM9, GEOM-Drugs	98.7	82.0	91.9	90.7
GCDM [83]	EGNN, Diffusion	QM9	98.7	85.7	94.8	93.3
MDM [84]	EGNN, VAE, Diffusion	QM9, GEOM-Drugs	99.2 [85]	89.6 [85]	98.6	94.6
JODO [85]	EGNN, Diffusion	QM9, GEOM-Drugs	99.2	93.4	99.0	96.0
MiDi** [86]	EGNN, Diffusion	QM9, GEOM-Drugs	99.8	97.5	97.9	97.6
GeoLDM** [81]	VAE, Diffusion	QM9, GEOM-Drugs	98.9	89.4	93.8	92.7

Table 1. An overview of relevant molecular generation models. All benchmarking metrics are self-reported unless otherwise noted. All metrics are evaluated with the QM9 dataset. For models with multiple variations, the highest-performing version was selected. [**] represents the current SOTA. As MiDi and MDM use slightly different evaluation conditions, their results are not fully comparable.

- **QM9** [77] - *Quantum Machines 9*, contains small stable molecules pulled from the larger chemical universe database GDB-17
- **GEOM-Drug** [78] - *Geometric Ensemble of Molecules*, contains more complex, drug-like molecules, often used to test scalability beyond the simpler molecules of QM9

Task

The target-agnostic molecule design task is as follows: given no input, generate a set of novel, valid, and stable molecules.

Metrics

The most general task within this field is unconditional molecule generation: after training on a set of existing molecules, generate a new set of valid, stable molecules. Validity, stability, and other commonly used metrics are formally defined below. All of these metrics can be evaluated using either QM9 or GEOM-Drug as training sets.

- **Atom Stability** - The percentage of atoms with the correct valency
- **Molecule Stability** - The percentage of molecules whose atoms are all stable
- **Validity** - The percentage of stable molecules that are considered valid, often evaluated by RDKit
- **Uniqueness** - The percentage of valid molecules that are unique (not duplicates)
- **Novelty** - The percentage of molecules not contained within the training dataset
- **QED** [30] - *Quantitative Estimate of Drug-Likeness*, a formulaic combination of a variety of molecular properties that collectively estimate how likely a molecule is to be used for pharmaceutical purposes

Note that the novelty metric is sometimes omitted, as argued by Vignac et al. [79], who contend that QM9 is an exhaustive set of all molecules with up to nine heavy atoms following a predefined set of constraints. Therefore, any “novel” molecule would have to break one of these constraints, making novelty a poor indicator of performance. While QED is a well-established metric for the evaluation of drug-likeness and is expected to see expanded usage in the future, many current models have focused solely on generating valid molecules and do not report performance on QED.

In addition, models are often evaluated on conditional molecule generation: given a desired chemical property, they generate molecules that fit this property. To test this ability, a property classifier network ϕ_c is trained on half of the QM9 dataset, while the model is trained on the other half. ϕ_c is then evaluated on the model’s generated molecules, and the mean absolute error between the target property value and

the evaluated property value is calculated. Below are the six molecular properties considered:

- α - *Polarizability*, or the tendency of a molecule to acquire an electric dipole moment when subjected to an external electric field, measured in cubic Bohr radius (Bohr^3)
- ϵ_{HOMO} - *Highest Occupied Molecular Orbit Energy*, measured in millielectron volts (meV)
- ϵ_{LUMO} - *Lowest Unoccupied Molecular Orbit Energy*, measured in millielectron volts (meV)
- $\Delta\epsilon$ - Difference between ϵ_{HOMO} and ϵ_{LUMO} , measured in millielectron volts (meV)
- μ - *Dipole moment*, measured in debyes (D)
- C_v - *Molar heat capacity* at 298.15 K , measured in calories per Kelvin per mole $\frac{cal}{mol K}$

Models

Approaches to the molecular generation task have seen significant shifts over the past few years, transitioning from 1D SMILES strings to 2D connectivity graphs, then to 3D geometric structures, and finally to incorporating both 2D and 3D information.

Early methods like Character VAE (CVAE) [87], Grammar VAE (GVAE) [88], and Syntax-Directed VAE (SD-VAE) [89] apply VAEs to 1D SMILES string representations of molecule graphs. While 1D SMILES strings can be deterministically mapped to molecular graphs, SMILES falls short in quality of representation – two graphs with similar chemical structures may end up with very different SMILES strings, making it harder for models to learn these similarities and patterns [90].

Junction Tree VAE (JTVAE) [90] was the first model to address this issue by generating 2D graph structures directly. JTVAE generates a tree-structured scaffold and then converges this scaffold into a molecule using a graph message passing network. This approach allows JTVAE to iteratively expand its molecule and check for validity at each step, resulting in considerable performance improvement over previous SMILES-based methods.

2D graph methods like JTVAE still fall short due to the lack of 3D input; because binding and interaction with other molecules/proteins rely heavily on 3D conformations, models that do not consider 3D information cannot properly represent and optimize properties like binding affinity. Thus, more recent developments include models that incorporate 3D information. Earlier 3D-based methods like E-NF [82] and G-SchNet [80] approached the molecular generation problem with flow-based methods or autoregressive methods (in particular, G-SchNet uses the SchNet architecture developed by Schutt et al. [67]). More recently, a wave of diffusion-based models operate on 3D point clouds, taking advantage of E(3) equivariance and demonstrating superior performance.

Model	Atom Stb. (% , \uparrow)	Mol Stb. (% , \uparrow)	Valid (% , \uparrow)	Val/Uniq. (% , \uparrow)
EDM [91]	81.30	\	\	\
MDM [84]	\	62.20	99.50	99.00
MiDi [86]	99.80	91.60	77.80	77.80
GeoLDM [81]	84.40	\	99.30	\

Table 2. Molecular generation models evaluated on the larger GEOM-Drugs dataset. All metrics are self-reported. As MiDi uses slightly different evaluation conditions, its results are not fully comparable.

Task (\downarrow)	α	Δ_e	ϵ_{HOMO}	ϵ_{LUMO}	μ	C_v
Units	$Bohr^3$	meV	meV	meV	D	$\frac{cal}{mol} K$
EDM [91]	2.76	655	356	584	1.111	1.101
GCDM [83]	1.97	602	344	479	0.844	0.689
MDM [84]	1.591	44	19	40	1.177	1.647
GeoLDM [81]	2.37	587	340	522	1.108	1.025

Table 3. Molecular generation models evaluated on the conditional molecule generation task. All metrics are self-reported.

EDM [91] provided an initial baseline for the application of diffusion, applying a standard diffusion process to an equivariant GNN with atoms represented as nodes with variables for both scalar features and 3D coordinates. While autoregressive models require an arbitrary ordering of the atoms, diffusion-based methods like EDM are not sequential and do not need such ordering, reducing a dimension of complexity and thus improving efficiency.

Many subsequent models compared themselves with EDM as a baseline on the molecule generation task, seeking to improve upon its performance by adding additional considerations and adjustments. GCDM [83] implements a crossover between geometric deep learning and diffusion, using a geometry-complete perceptron network to introduce attention-based geometric message-passing. While both EDM and GCDM have already demonstrated massive performance improvements, both models still struggle with both large-molecule scalability and diversity in the generated molecules. MDM [84] addressed the scalability issue by pointing out the lack of consideration for interatomic relations in EDM and GCDM. MDM separately defines graph edges for covalent bonds and for Van der Waals forces (dependent on a physical distance threshold τ) to allow for thorough consideration of interatomic forces and local constraints. In addition, MDM addressed the diversity issue by introducing an additional distribution-controlling noise variable in each diffusion step. While previous diffusion models operated directly in the complex atomic feature space, GeoLDM [81] applies VAEs to map molecule structures to a lower-dimensional latent space for its diffusion. This latent space has a smoother distribution and lower dimensionality, leading to higher efficiency and scalability for large molecules. In addition, conditional generation is improved, as specified chemical properties are more clearly defined within latent spaces than they are in raw format.

While previous models learned exclusively from either 2D or 3D representations, a new wave of models recognize the need for both: a molecule’s 2D connectivity structure is necessary to determine bond types and gather information about chemical properties and synthesis, while the 3D conformation is crucial for its interaction and binding affinity with other molecules. By jointly learning and generating both representations, models can maximize the amount of chemically relevant information and produce higher-quality molecular samples. The Joint 2D and 3D Diffusion Model (JODO) [85] uses a geometric graph representation to capture both 3D spatial information and connectivity information, applying score SDEs to this joint

representation while proposing a diffusion graph transformer to parameterize the data prediction model and avoid the loss of correlation after noise is independently added to each separate channel. MiDi [86] uses a similar graph representation but instead applies a DDPM. It proposes a “relaxed” EGNN, which improves upon the classical EGNN architecture by exploiting the observation that translational invariance is not needed in the zero center-of-mass subspace. An full overview of the developments described in this section can be seen in Figure 3.

As shown in Table 1, diffusion-based methods demonstrate significant improvements over previous methods, all achieving over 98.5% in atom stability. However, some models fall behind when extended to the larger GEOM-Drugs dataset, as shown in Table 2, where MiDi distinguishes itself for its capability to generate more stable complex molecules, albeit at the expense of validity. Table 3 illustrates that MDM and GCDM excel at conditional generation tasks, with the former model achieving the best performance in four out of six tasks and the latter outperforming the remaining two. Overall, current models demonstrate high performance on the QM9 dataset, but there is room for improvement when dealing with the more complex molecules found in the GEOM-Drugs dataset.

Target-Aware Molecule Design

Overview

Contrasting target-agnostic molecule design, target-aware design involves generating molecules based on specific biological targets. Within target-aware design, two primary approaches exist: ligand-based drug design (LBDD) and structure-based drug design (SBDD). LBDD models often utilize the amino acid sequences of target proteins, leveraging the characteristics and features of known ligands to build new molecules with similar properties. By contrast, SBDD models use the 3D structure of the target protein to design a corresponding molecular structure. LBDD models are most useful when the 3D structure is not experimentally available, but are limited in novelty because they only learn from existing bindings [44]. When the 3D structure of the target protein is available, SBDD models are generally preferred, as they consider crucial 3D information.

Datasets

The following datasets are used for target-aware molecule design. CrossDocked2020 [92] is currently the most heavily used, as the cross-docking technique allows for the generation of combinatorially large quantities of data by “mixing and

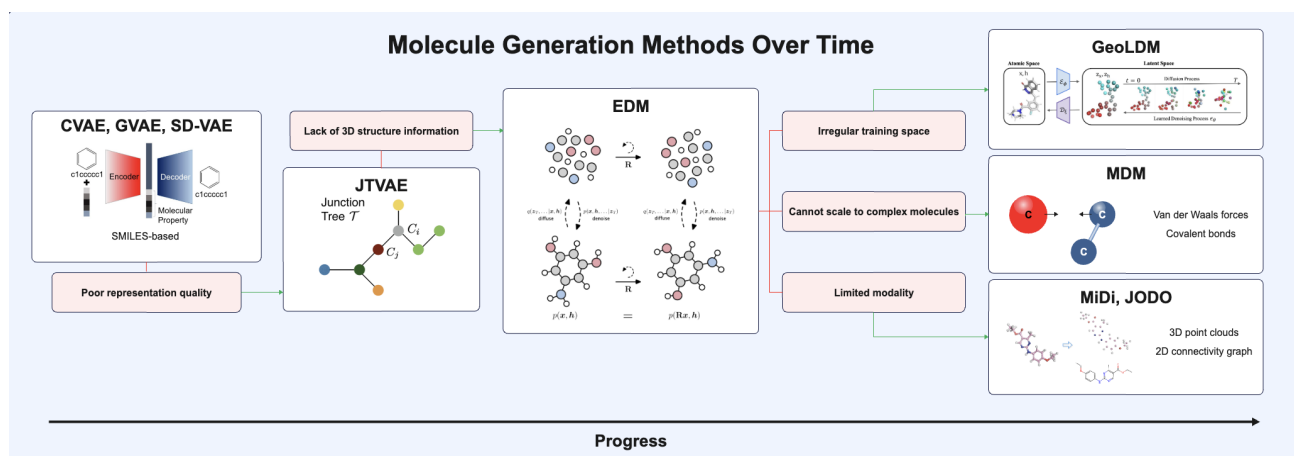


Fig. 3. An overview of the progress in target-agnostic molecule design over time. Shortcomings of previous models are highlighted in red, with subsequent models solving these shortcomings through novel design choices. Images used from [87, 91, 90, 81, 84, 85].

matching” similar ligand-protein pairs (22.5M compared to 40K in Binding MOAD [93]).

- **CrossDocked2020** [92] - Contains ligand-protein complexes generated by cross-docking within clusters of similar binding sites called “pockets”
- **ZINC20** [94] - Fully enumerated dataset of possible ligands
- **Binding MOAD** [93] - *Binding Mother of All Databases*, a subset of PDB [95] containing experimentally determined protein-ligand pairings

Task

Given input target information, typically in the form of protein amino acid sequences in LBDD and protein 3D structure in SBDD, these approaches generate molecules that exhibit high binding affinity and potential interactions with this target.

Metrics

Target-aware molecule design utilizes the following metrics. Beyond affinity/applicability metrics, an additional consideration for diversity is considered, as a diverse array of potential options for a given target can provide more flexibility in the drug development process.

- **Vina Score** [96] - Scoring function supported by the Vina platform that returns a weighted sum of atomic interactions and is useful for docking
- **Vina Energy** [96] - Energy prediction by the Vina platform that is used to measure binding affinity
- **High Affinity Percentage** - Percentage of molecules with lower Vina energy than the reference (ground-truth) molecule when binding to the target protein
- **QED** [30] - *Quantitative Estimate of Drug-Likeness*, which is also used in target-agnostic generation (see page 6)
- **SAscore** [97] - *Synthetic Accessibility Score*, a formulaic combination of molecular properties that determine how easy a molecule is to create in a real lab setting
- **Diversity** - The diversity of generated molecules for each specific binding site, measured by Tanimoto similarities [98] between pairs of Morgan fingerprints

Models

LBDD models incorporate transformer architectures to generalize properties of learned ligands. For example, DrugGPT [99] is a recent autoregressive model that uses transformers

to train numerous protein-ligand pairs. In their model, the ligand SMILES and protein amino acid sequence are tokenized for training, and the model produces viable SMILES ligand outputs. Generally, with improving protein structure prediction methods (see page 10) and increasing access to structural information as a whole, SBDD methods have become more prevalent than LBDD methods; thus, we explore SBDD methods below in more detail.

LiGAN [100] introduces the idea of a 3D target-aware molecule output, fitting molecules into grid formats for learning with a CNN and training the model under a VAE framework. Pocket2Mol [101] places more emphasis on the specific “pockets” on the target protein to which the molecules bind, using an EGNN and geometric vector MLP layers to train on graph-structured input. Luo et al. [102] directly model the probability of atoms occurring at a certain position in the binding site, taking advantage of invariance through the SchNet [67] architecture.

Recent SBDD models have also popularized the use of diffusion models. TargetDiff [103] performs diffusion on an EGNN (with many similarities to EDM [91]) to learn the conditional distribution. To optimize the binding affinity, Guan et al. note that the flexibility of atom types should be low, which is reflected by the entropy of the atom embedding. Schneuing et al. [104] propose DiffSBDD, which includes two sub-models: DiffSBDD-cond and DiffSBDD-inpaint. DiffSBDD-cond is a conditional DDPM that learns a conditional distribution in a similar way as TargetDiff. In our benchmarking, we focus on the higher performing model, DiffSBDD-inpaint, which applies the inpainting approach (traditionally applied to filling parts of images) by masking and replacing segments of the ligand-protein complex.

As shown in Table 4, DiffSBDD leads in Vina score and diversity, while TargetDiff leads in high affinity. Interestingly, diffusion-based methods seem to be outperformed by the MLP used in Pocket2Mol when it comes to drug-like metrics like QED and SA. However, Guan et al. [103] note that adjustments to TargetDiff, such as switching to fragment-based generation or predicting atom bonds, could improve performance on QED and SA.

Model	Type of Model	Dataset	Vina Score	High Affinity (%)	QED	SA	Diversity
Luo et al. [102]	SchNet	CrossDocked2020	-6.344	29.09	-0.525	0.657	0.720
LiGAN [100]	CNN, VAE	CrossDocked2020	-6.144 [102]	21.1 [103]	0.39 [103]	0.59 [103]	0.66 [103]
Pocket2Mol** [101]	EGNN, MLP	CrossDocked2020	-5.14 [103]	48.4 [103]	0.56 [103]	0.74 [103]	0.69 [103]
TargetDiff** [103]	EGNN, Diffusion	CrossDocked2020	-6.3	58.1	0.48	0.58	0.72
DiffSBDD** [104]	EGNN, Diffusion	CrossDocked, Bind. MOAD	-7.333	\	0.467	0.554	0.758

Table 4. An overview of relevant target-aware molecular generation models. All benchmarking metrics are self-reported unless otherwise noted. [**] represents the current SOTA. As each paper uses slightly different benchmarking methods, their results may not be fully comparable.

Molecular Conformation Generation

Overview

While learning on graph-structured data has found success in molecular generation, recent models have demonstrated that incorporating 3D information is crucial to understanding various chemical properties such as binding affinity. However, deriving a 3D structure from a 2D connectivity graph is nontrivial; given a 2D graph, there are numerous ways to construct a 3D arrangement of molecules that still adheres to the same connectivity structure. Two molecules with the same chemical formula but different 3D arrangements are called conformers (or conformational isomers).

Datasets

The following datasets are used for conformation generation. Note that while GEOM-QM9 [78] is created with the same molecules as in the general QM9 [77] dataset, the GEOM-QM9 dataset contains a complete set of representative conformers for each molecule. QM9 only provides singular 3D structures and cannot be applied to conformation generation.

- **GEOM-QM9** [78] - Set of all conformers for each molecule in QM9. Reference conformations are created through a standardized process using density functional theory.
- **GEOM-Drugs** [78] - Conformers for more complex drug-like molecules, also used in general molecule generation (see page 5)
- **ISO17** [67] - Set of molecular conformations for all molecules with the chemical formula $C_7O_2H_{10}$

Task

Given a 2D molecule connectivity graph, this approach generates a set of stable 3D conformations that correspond to the given connectivity structure.

Metrics

While other tasks like property prediction are often evaluated on models in this field, we focus on generative tasks like conformation generation. The following metrics are used to judge the quality of the conformation generation task. Intuitively, COV measures the diversity of the generated sample, while MAT measures quality/accuracy.

- **COV** [105] - *Coverage*, a percentage of how many ground-truth conformations are “covered” (below a threshold root-mean-square deviation (RMSD) with some generated conformation, typically 0.5Å for QM9 and 1.25Å for Drugs).
- **MAT** [105] - *Matching*, the average RMSD between each generated conformation and the closest ground-truth conformation.

Models

Mansimov et al. propose a conditional variational graph autoencoder (CVGAE) [106] for molecule generation, directly applying a GNN to learn atom representations and generate

3D coordinates. GraphDG [107] improves upon this by modeling distance geometry between atoms, which incorporates rotational and translational invariance (i.e., two identical molecules are treated equally under transformation). Conditional graph continuous flow (CGCF) [105] applies a flow-based approach to model the distance geometry, combining this with an (EBM) as a “tilting” term for mutual enhancement. GeoMol [108] argues that methods solving for distance geometries are flawed, as creating distance matrices leads to overparameterization, and important geometric features like torsional angles are not directly modeled. To address this, GeoMol uses an MPNN to individually predict the local structure for each atom, allowing for a more direct representation of neighboring features. ConfGF [109] pulls ideas from force field methods in molecular dynamics, directly learning gradient fields of the log density for atom coordinates, using a GIN [110] to adjust for rotational and translational invariance. Dynamic graph score matching (DGSM) [111] extends the ideas of ConfGF by constructing dynamic graphs to incorporate long-range atomic interactions (instead of relying on static input graphs that only consider chemical bonds). GeoDiff [112] uses an Euclidean space diffusion process, treating each atom as a particle. GeoDiff incorporates Markov kernels that preserve equivariance, as well as roto-translational invariance through their proposed graph field network (GFN) layer, which draws inspiration from the eGNN architecture [62]. Torsional Diffusion [113] uses score-based diffusion in the space of torsion angles, which allows for improved representation and fewer denoising steps than GeoDiff.

As shown in Table 5, Torsional Diffusion appears to outperform all other models, with DGSM and GeoDiff also exhibiting competitive performance. Notably, methods that focus on torsional angles seem to outperform other methods with similar architectures: GeoMol outperforms distance-graph methods like GraphDG and CGCF, while Torsional Diffusion outperforms GeoDiff.

Protein

Task Background

Proteins are large biomolecules that contain one or more long chains of amino acids. Each amino acid is a molecular compound that contains both an amino (-NH₂) and a carboxylic acid (-COOH) [114]. While there are over 500 naturally occurring amino acids, only 22 are proteinogenic (“protein-building”) and thus relevant to the protein generation task [115]. Thus, in addition to 3D structural representations, proteins can be represented through their amino acid sequences, assigning each amino acid a letter label and representing each long chain as a string of labels. This sequential representation for amino acids mirrors the sequence structure of human language, allowing for natural language models to be applied in ways that would not be possible for the previously

Model	Type of Model	Dataset	GEOM-QM9		GEOM-Drugs	
			COV (% , \uparrow)	MAT (\AA , \downarrow)	COV (% , \uparrow)	MAT (\AA , \downarrow)
CVGAE [106]	VAE, MPNN	QM9, COD, CSD	0.09 [111]	1.6713 [111]	0.00 [111]	3.0702 [111]
GraphDG [107]	VAE	ISO17	73.33 [111]	0.4245 [111]	8.27 [111]	1.9722 [111]
CGCF [105]	Flow, EBM	G-QM9, G-Drugs, ISO17	78.05 [112]	0.4219 [112]	53.96 [112]	1.2487 [112]
ConfGF [109]	GIN, Diffusion	G-QM9, G-Drugs	88.49 [111]	0.2673 [111]	62.15 [111]	1.1629 [111]
GeoDiff** [112]	GFN, Diffusion	G-QM9, G-Drugs	90.07	0.209	89.13	0.8629
GeoMol [108]	MPNN	G-QM9, G-Drugs	71.26 [112]	0.3731 [112]	67.16 [112]	1.0875 [112]
DGSM** [111]	MPNN, Diffusion	G-QM9, G-Drugs	91.49	0.2139	78.73	1.0154
Torsional** [113]	Diffusion	G-QM9, G-Drugs, G-XL	92.8	0.178	72.7*	0.582

Table 5. An overview of relevant molecule conformation generation models. All benchmarking metrics are self-reported unless otherwise noted. GEOM-QM9 and GEOM-Drugs are denoted as G-QM9, and G-Drugs for brevity. [*] Torsional Diffusion uses a threshold of 0.75 \AA instead of 1.25 \AA to calculate coverage on GEOM-Drugs, leading to a deflated score. Notably, Torsional Diffusion outperforms GeoDiff and GeoMol when tested on this threshold. [**] represents the current SOTA.

discussed molecule generation task. Within protein generation, several generative subtasks can be defined. *Representation learning* involves creating meaningful embeddings for protein inputs, which improves the data space for other models to train on. *Structure prediction* involves the generation of a protein structure from its corresponding amino acid sequence, historically a challenging task due to the vast conformational space. Finally, *protein generation* refers to creating proteins from scratch, which forms the core of the *de novo* design task.

We also briefly discuss antibody generation due to its high relevance within the protein generation field. In particular, antibodies are Y-shaped proteins used by the immune system to identify and bind to bacteria known as antigens. While many protein design models use multiple sequence alignment (MSA) to map evolutionary relationships between related sequences, MSAs are not always available for antibody sequences, and antibody-specific models cannot rely on this input. Additionally, binding regions are specifically defined for antibodies, contained within six complementarity-determining regions (CDRs). The CDR-H3 region is particularly diverse and complex, leading to a specialized task for the reconstruction of this region, known as CDR-H3 generation. Further discussion of antibody generation can be found in the appendix on page 23.

Protein Representation Learning

Overview

Protein representation learning involves learning embeddings to convert raw protein data into latent space representations, thereby extracting meaningful features and chemical attributes. Specifically, given a protein $x = [o_1, o_2, \dots, o_L]$, where each o_i represents an amino acid (sequence-based) or atom coordinate (structure-based), the goal is to learn an embedding $z = [h_1, h_2, \dots, h_L]$, where each $h_i \in \mathbb{R}^d$ represents a d -dimensional token representation for amino acid o_i . Although representation learning is not a generative task on its own, these embeddings create “richer” data spaces for other generative models to train on. Hence, we briefly discuss them here. For a more in-depth analysis of protein representation learning models, please refer to the appendix on page 22.

Protein representation learning models often draw inspiration from natural language processing, leveraging the language-like structures of amino acid strings. ProtBERT [116] applies a BERT model [69], a pre-trained language model, to amino acid sequences, treating each residue as a word. ESM-1B [117] trains a deep transformer with 33 layers and 650 million parameters, using the masked language modeling (MLM) objective. ESM-1b considers residue contexts across the entire sequence through

its stacked attention layers. Its complexity and size enable it to outperform other SOTA models on a wide range of tasks, as shown below.

Notably, ProtBERT is used in ProteinVAE [118] for protein generation, and an improved ESM-1b (ESM-2) is used in ESMFold [119] for protein structure prediction, both of which are discussed in later sections.

Antibody Representation Learning

Within protein representation learning, a class of models focuses on pretraining specifically on antibody sequence data. Models in this field similarly draw inspiration from language models, with AntiBERTy [120] using a BERT-based model and more recent models like PARA [121] and AntiBERTa [122] using improved DeBERTa [123] and RoBERTa [124] architectures. Analogous to the general protein case, antibody-specific representation learning models aim to improve antibody-specific structure prediction and generation. For a more detailed analysis of various antibody representation learning methods, refer to the appendix on page 24.

Structure Prediction

Overview

Generating 3D structures of proteins from their amino acid sequence is a challenging and important task in drug design. Historically, *de novo* modeling has fallen short due to a lack of computational power and the difficulty of finding structures in the vast conformational space. New research in computational modeling has used various deep learning architectures to discover information from the amino acid sequences to generate accurate 3D structures. Current models have achieved impressive accuracy in structure prediction, but there is room for improvement in terms of speed and scale.

Datasets

Unlike many of the other fields mentioned previously, the field of protein structure prediction benefits from a widely standardized benchmarking task through the Critical Assessment of Protein Structure Prediction (CASP). CASP conducts biennial testing on models using solved protein structures that have not been released to PDB.

- **PDB** [95] - *Protein Data Bank*, a central archive for all experimentally determined protein structures, widely used in almost all protein structure-related tasks
- **CASP14** [125] - *14th Critical Assessment of Protein Structure Prediction*, a set of unreleased PDB structures used to create a standardized blind testing environment

Model	Type of Model	Dataset	CAMEO				CASP14	
			RMSD (Å, ↓)	TMScore (↑)	GDT-TS (↑)	IDDT (↑)	TMScore (↑)	
AlphaFold2** [130]	Transformer	CASP14	3.30 [131]	0.87 [131]	0.86 [131]	0.90 [131]	0.38 [119]	
RoseTTAFold [132]	Transformer	CAMEO, CASP14	5.72 [131]	0.77 [131]	0.71 [131]	0.79 [131]	0.37 [119]	
ESMFold [119]	Transformer	CAMEO, CASP14	3.99 [131]	0.85 [131]	0.83 [131]	0.87 [131]	0.68	
EigenFold [131]	Diffusion	CAMEO	7.37	0.75	0.71	0.78	\	

Table 6. An overview of relevant protein structure prediction models. All metrics are self-reported unless otherwise noted. Scores are provided as mean performance on single-structure tasks. IDDT represents the IDDT metric computed specifically using coordinates for the alpha carbon of each residue. [**] denotes the current SOTA.

- **CAMEO** [126] - *Continuous Automated Model Evaluation*, a complement to CASP that conducts weekly blind tests using around 20 pre-released PDB targets (to provide more continuous feedback, as CASP is biennial)

Task

Given a protein amino acid sequence, the goal is to generate a set of 3D point coordinates for each amino acid residue.

Metrics

Models are evaluated by comparing each protein’s ground-truth structure with the generated structure. Three different approaches are taken to evaluate structural similarity:

- **RMSD** - *Root-Mean-Square Deviation*, directly compares ground-truth positions with generated positions for each amino acid. If each δ_i denotes the distance between each ground truth and generated amino acid position, with N total amino acids, we have:

$$\text{RMSD} = \sqrt{\frac{1}{N} \sum_{i=1}^N \delta_i^2}$$

- **GDT-TS** [127] - *Global Distance Test-Total Score*, finds the most optimal superposition between two structures, searching for the highest number of corresponding residues that are within a distance threshold from each other. The GDT-TS aims to represent global fold similarities.
- **TM-score** [128] - *Template Modeling score*, a similarity scoring formula that adjusts the GDT metric, normalizing for protein sequence length to avoid dependency on protein size, evaluating all residues beyond just those within the proposed cutoff for a more cohesive score. The TM-score aims to represent both global fold and local structural similarities.
- **IDDT** [129] - *Local-Distance Difference Test*, a superpos.-free metric based on local distances between atoms. For each atom pair, its local distance is “preserved” if the generated local distance is within a given threshold of the ground-truth distance, and the proportion of preserved distances is calculated. The IDDT can protect against artificially unfavorable scores when considering flexible proteins with multiple domains.

Models

AlphaFold2 [130] is a landmark model that uses deep learning techniques to compete with experimental methods. AlphaFold2 integrates numerous layers of transformers in an end-to-end approach. The transformers incorporate information from the MSA and pair representations to explore the folding space, potential orientations of amino acids, and overall structure based on pairwise distances. The MSA aligns multiple related protein sequences to create a 2D representation that informs the transformer architecture. Additionally, AlphaFold2

employs invariant point attention (IPA) for spatial attention, while the transformer captures interactions along the chain structure. Notably, AlphaFold2 introduces novel constraints from experimental data, which record probable distances between residues, preferred orientations between residues, and likely dihedral angles for the covalent bonds in the backbone.

Proposed in 2020, trRosetta [133], i.e., transform-restrained Rosetta, is another model that uses a deep residual network with attention mechanisms. Upon inputting MSA information, trRosetta predicts distances and orientations for residue pairs, which are then utilized to construct the 3D structure using a Rosetta protocol. Despite their advancements, both trRosetta and AlphaFold2 face several challenges, including their reliance on the MSA representation, limitations to natural proteins, and high computational requirements. Recently, RoseTTAFold [132], which replaced trRosetta [133], demonstrated performance comparable to AlphaFold2 based on CASP14 test data. Importantly, RoseTTAFold can generate samples within 10 minutes, which is around 100 times faster than AlphaFold2. RoseTTAFold employs a three-track neural network that simultaneously learns from 1D sequence-level, 2D distance map-level, and 3D backbone coordinate-level information with attention mechanisms integrated throughout. RoseTTAFold exhibits robust performance in predicting protein complexes, whereas AlphaFold2 excels primarily for single protein structure prediction.

Building on these techniques, ESMFold [119] is a language model that predicts protein structure by leveraging ESM-2 representations. The output embeddings from ESM-2 are passed to a series of self-attending “folding blocks.” A structure module, featuring an SE(3) transformer architecture, generates the final structure predictions. Since ESMFold uses ESM-2 representations instead of MSA representations, this model offers faster processing with competitive scores on CAMEO and CASP14. EigenFold [131] is another model that applies diffusion models to generate protein structures. The model represents the protein as a system of harmonic oscillators. Then, the structure can be projected onto the eigenmodes of that system during the forward process. In the reverse process, the rough global structure is sampled before refining local details. As a score-based model, EigenFold is not as computationally intensive but still underperforms in accuracy and range compared to other models.

Antibody Structure Prediction

A class of models has also been developed specifically catering to antibody structure prediction. As discussed previously, MSA alignment cannot be used for antibody input, rendering general models like AlphaFold highly inefficient and slow in the context of antibody prediction. IgFold [134] uses sequence embeddings from AntiBERTy [120] and invariant point attention to predict

antibody structures, achieving SOTA generation speed with comparable accuracy to other models in the field. tFold-Ab [135] performs comparably to IgFold, generating full-atom structures more efficiently by reducing reliance on external tools like Rosetta energy functions. For a more in-depth analysis of the datasets, task definition, metrics, and performance, refer to the appendix on page 24.

Protein Generation

Overview

Like molecule generation, generating novel proteins from scratch can directly expand the library of available proteins capable of performing highly complex and versatile functions. While other areas such as structure prediction and representation learning contribute to the overall drug design process, protein generation lies at the core of *de novo* design, where new protein structures and sequences can be generated entirely from scratch.

Notably, we observe a similar distinction between structure and sequence as seen in molecule generation. Some models generate 1D amino acid sequences, while others directly generate 3D structures, with some co-designing both 1D sequences and 3D structures.

Datasets

Models in this field utilize the following datasets:

- **PDB** [95] - *Protein Data Bank*, a comprehensive protein structure dataset (see page 10)
- **AlphaFoldDB** [136] - *AlphaFold Database*, an expanded protein structural dataset created by using AlphaFold2 to predict structures for corresponding sequences in the UniRef dataset
- **SCOP** [137] - *Structural Classification of Proteins*, a classification of proteins by homology and structural similarity. SCOP has been updated several times to include additional categorizations and features, with many recent models using the extended SCOPe [138] database.
- **CATH** [139] - A classification of protein domains (sub-sequences that can fold independently) into a hierarchical scheme with four levels: class (C), architecture (A), topology (T), and homologous superfamily (H). Using their classification, the authors also provide a diverse set of proteins that have minimal overlap and sequence similarity.

Tasks

The protein generation task involves designing a protein sequence/structure either from scratch or based on existing context. For structure-based methods, many models focus on the backbone structure of these proteins, which involves generating the backbone atoms for each amino acid (nitrogen, alpha-carbon, carbonyl, and oxygen atom). External tools like Rosetta [140] can be used for side-chain packing, generating the remaining atoms.

- **Context-Free Generation** - Given no input, the goal is to generate a protein sequence and/or structure with high designability. This task is evaluated using the self-consistency TM (scTM) score.
- **Context-Given Generation** - This is an inpainting task for proteins. Given a motif (a set of existing amino acid residues for a native protein), the goal is to accurately fill in the missing residues according to the native protein, which is evaluated using a variety of similarity metrics like AAR, PPL, and RMSD.

Metrics

For context-free generation, high “designability” is generally determined by the ability of a structure to be generated by a corresponding amino acid sequence. While lab testing is optimal, this is not always feasible, so the folding process is simulated by other generative models. Thus, Trippe et al. [141] proposed the scTM approach, which includes the following steps: a proposed structure is fed into a sequence-prediction model (typically ProteinMPNN [142]) to produce a corresponding amino acid sequence, and then fed back into a structure prediction model (typically AlphaFold2 [130]) to produce a sample structure. The TM-score (see page 10) between the generated structure and this sample structure is calculated.

- **scTM** [141] - *Self-consistency TM-score*, an approach proposed by Trippe et al. to simulate the folding process, described in detail above. Scores of scTM > 0.5 are typically considered designable, so the percentage of generated structures with scTM > 0.5 is often reported.
- **scRMSD** - *Self-consistency RMSD*, identical to the scTM but uses RMSD instead of the TM-score for evaluation. A score of scRMSD < 2 is typically used as a cutoff.
- **AAR** - *Amino acid recovery*, a comparison between the ground truth and the generated amino acid sequences. The AAR is also measured in antibody representation learning (see page 24).
- **PPL** - *Perplexity*, an exponentiation of cross-entropy loss, representing the inverse likelihood of a native sequence appearing in the predicted sequence distribution. For a series of N amino acids x_1, x_2, \dots, x_N , we can express perplexity as:

$$\text{PPL} = \exp\left(\frac{1}{N} \sum_{i=1}^N \log P(x_i | x_{<i})\right)$$

Perplexity is calculated individually for each protein in the test set and averaged to produce a final PPL value.

- **RMSD** - *Root-mean-square deviation*, measures distances between the ground truth and the generated residue coordinates. The RMSD is also used in protein structure prediction (see page 10).

Models

The first class of models primarily focuses on generating novel protein sequences. ProteinVAE [118] utilizes ProtBERT [116] to reduce raw input sequences into latent representations. It employs an encoder-decoder framework with position-wise multi-head self-attention to capture long-range dependencies in these sequences. ProT-VAE [152] uses a different pre-trained language model ProtT5NV [153]. It includes an inner family-specific encoder-decoder layer to learn parameters relevant to specific protein families. Conversely, ProteinGAN [154] uses a GAN architecture to generate protein sequences. The model’s efficacy is exemplified through the example of malate dehydrogenase, demonstrating its potential to generate fully functional enzyme proteins.

Another class of models focuses on generating novel protein structures. ProtDiff [141] represents each residue with 3D Cartesian coordinates and uses a particle filtering diffusion approach. However, 3D Cartesian point clouds do not mirror the folding process to create protein structures—FoldingDiff [144] instead uses an angular representation for the protein structure, which more closely mirrors the rotational energy-optimizing protein folding process. FoldingDiff treats the

Model	Type of Model	Dataset	Context-Free			Context-Given	
			scTM (% , \uparrow)	Design. (% , \uparrow)	PPL (\downarrow)	AAR (% , \uparrow)	RMSD (\AA , \downarrow)
LatentDiff [143]	EGNN, Diffusion	PDB, AFDB	31.6	\	\	\	\
FoldingDiff [144]	Diffusion	CATH	14.2 [143]	\	\	\	\
FrameDiff [145]	Diffusion	PDB	84	48.3 [146]	\	\	\
Genie [146]	Diffusion	SCOPe, AFDB	81.5	79.0	\	\	\
RFDiffusion** [147]	Diffusion	PDB	\	95.1 [146]	\	\	\
ProtDiff [141]	EGNN, Diffusion	PDB	11.8 [143]	\	\	12.47* [148]	8.01* [148]
GeoPro [148]	EGNN	PDB	\	\	\	43.41*	2.98*
ProtSeed [149]	MLP	CATH	\	\	5.6	43.8	\
Protpardelle [150]	Diffusion	CATH	85	\	\	\	\
GVP-GNN [151]	GVP-GNN	CATH	\	\	5.29 [149]	40.2 [149]	\

Table 7. An overview of relevant protein generation methods. “AFDB” refers to AlphaFoldDB. “Design” refers to designability, defined by Lin et al. [146], where any proteins with scRMSD < 2 and pLDDT > 70 (a local distance metric used in AlphaFold2 [130]) are considered designable. [*] denotes results tested specifically on β -lactamase metalloproteins extracted from PDB. [**] denotes the current SOTA.

protein backbone structure as a sequence of six angles representing orientations of consecutive residues. It denoises from a random, unfolded state to a folded structure using a DDPM and a BERT architecture. LatentDiff [143] initially uses an equivariant protein autoencoder with GNNs to embed proteins into a latent space. Subsequently, it uses an equivariant diffusion model to learn the latent distribution. This process is analogous to GeoLDM [81] for molecule design. Notably, LatentDiff’s sampling on its latent space is ten times faster than sampling on raw protein space.

The above models have shown relatively high performance in generating shorter proteins (up to 128 residues in length) but struggle with larger and more complex proteins [146]. To address longer protein structures, other methods use frame-based construction methods. This representation was initially demonstrated in the architecture of AlphaFold2 [130] in structure prediction, known as IPA. In this paradigm, each residue is represented by orientation-preserving rigid body transformations (reference frames), which can be consistently defined regardless of global orientation. This allows for a more generalized representation than a series of 3D point clouds. Genie [146] performs discrete-time diffusion using a cloud of frames determined by a translation and rotation element to generate backbone structures. During each diffusion step, Genie computes the Frenet-Senet frames and uses paired residue representations and IPA for noise prediction. FrameDiff [145] also parameterizes the backbone structures based on the frame manifold, using a score-based generative model. This approach establishes a diffusion process on $SE(3)^N$, the manifold of frames, invariant to translations and rotations. Then, the neural network predicts the denoised frame and torsion angle using IPA and a transformer model. Finally, RFDiffusion [147] combines the powerful structure prediction methods from RoseTTAFold with diffusion models to generate protein structures. RFDiffusion fine-tunes the RoseTTAFold weights and inputs a masked input sequence and random noise coordinates to iteratively generate the backbone structure. RFDiffusion also “self-conditions” on the predicted final structure, leading to improved performance. RFDiffusion is a large pre-trained model with significantly more parameters than the other two frame-based models, enabling it to outperform the other frame-based models.

A third class of models aims to co-design both protein sequence and structure simultaneously. GeoPro [148] uses an EGNN to encode and predict 3D protein structures, designing a separate decoder to decode protein sequences from these learned representations. Protpardelle [155] creates a “superposition” over the possible sidechain states and collapses

them during each iterative update step in the reverse diffusion process. The backbone is updated in each iterative step, while the sidechains are chosen probabilistically by another network to update. ProtSeed [149] uses a trigonometry-aware encoder that computes constraints and interactions from the context features and uses an equivariant decoder to translate proteins into their desired state, updating the sequence and structure in a one-shot manner. Anand et al. [156] use IPA as mentioned above, performing diffusion in frame space to efficiently generate protein sequences and structures. GVP-GNN [151] uses a simple yet novel geometric representation for all nodes in the system. Rather than individually encoding vector features (like relative node orientations) for each node, these features are directly represented as geometric vectors that transform accordingly alongside global transformations. This approach defines a global geometric orientation rather than independent features of each node.

For an overview of developments described in this section, see Figure 4. Note that as seen in molecule generation, we observe a progression from 1D-based (amino acid) models to 3D structure-based models to 1D/3D co-design; in addition, the field of protein design faces analogous questions of complexity scaling and latent space regularization.

Antibody CDR-H3 Generation

As mentioned previously, antibody generation primarily focuses on the generation of a particular region known as the CDR-H3 region. Similar to protein generation, models in CDR-H3 generation have transitioned from sequence-based methods like the LSTM used by Akbar et al. [157] to sequence-structure co-design pioneered by RefineGNN [158] through iterative refinement. Notably, some models extend beyond the CDR-H3 generation task, aiming to tackle multiple parts of the antibody pipeline at once. dyMEAN [159] is an end-to-end method incorporating structure prediction, docking, and CDR-H3 generation into a singular model. For a more in-depth analysis of datasets, task definition, metrics, and performance, refer to the appendix on page 25.

Current Trends

The drug design process, marked by a history of high complexity and cost, is poised for a transformative shift fueled by generative AI. AI-based methods are driving faster development and reducing costs, resulting in more effective and accessible pharmaceuticals for the public. Within the realm of generative AI, a notable shift has occurred; the emergence of GNNs and graph-based methods has fueled the transition from sequence-based approaches to structure-based approaches,

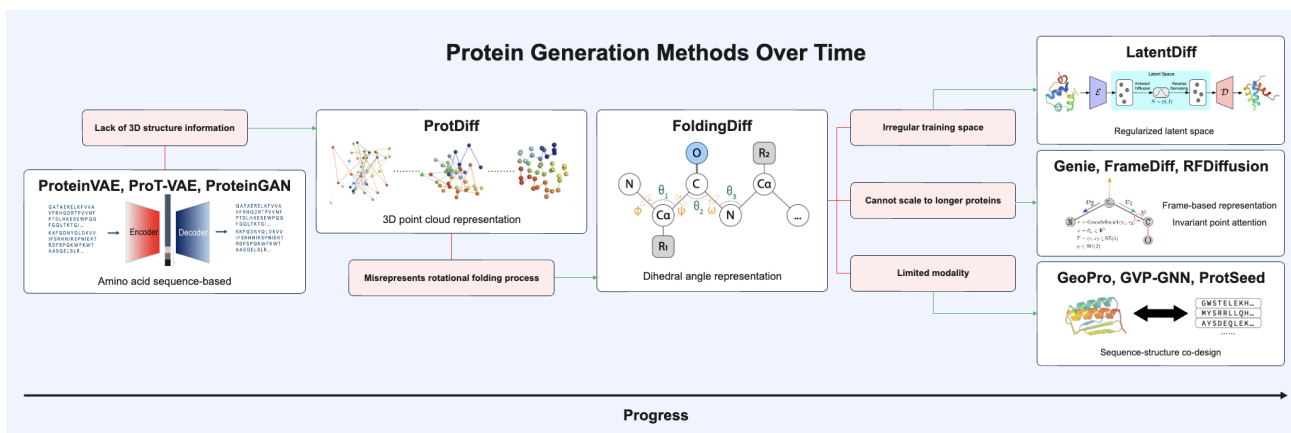


Fig. 4. An overview of the progress in protein generation over time. Shortcomings of previous models are highlighted in red, with subsequent models solving these shortcomings through novel design choices. Images used from [152, 141, 144, 143, 145, 149].

ultimately leading to the integration of both sequence and structure in generation tasks.

Within the field of molecular generation, we are witnessing the recent dominance of graph-based diffusion models. These models take advantage of $E(3)$ equivariance to achieve SOTA performance, with leaders like GeoLDM and MiDi excelling in target-agnostic design, and TargetDiff, Pocket2Mol, and DiffSBDD excelling in target-aware design. Finally, Torsional Diffusion outperforms all counterparts in molecular conformation generation. Additionally, we observe a shift from sequence to structural approaches in target-aware molecule design, where SBDD approaches demonstrate clear advantages over LBDD approaches, which operate with amino acid sequences.

Within protein generation, a shift from sequence to structure is evident, as exemplified by the emergence of structure-based representation learning models like GearNET. These models leverage established sequence-based representation models such as ESM-1B and UniRep, recognizing the importance of 3D structural information in the protein generation process. AlphaFold2 remains a clear SOTA model for structure prediction. Similar to molecule generation, a wave of diffusion models are now tackling the protein scaffolding task, with RFDiffusion emerging as the top-performing model.

Challenges and Future Directions

While the prospects for generative AI in drug design are promising, several issues must be addressed before we can embrace ML-driven *de novo* drug design. The main areas for improvement include increasing performance in existing tasks, defining more applicable tasks within molecule, protein, and antibody generation, and exploring entirely new areas of research.

Current generative models still struggle with a variety of tasks and benchmarks. Within molecule generation, we face the following challenges:

- **Complexity** - Models generate high frequencies of valid and stable molecules when trained on the simple QM9 dataset but struggle when trained on the more complex GEOM-Drugs dataset.
- **Applicability** - More applicable tasks like protein-molecule binding are especially challenging, and current models

still struggle with generating molecules with high binding affinity for targets.

- **Explainability** - All methods discussed are fairly black-box and abstract; existing models do not reveal aspects like “important” atoms or structures, and explainable AI in molecule generation is undeveloped as a whole.

Within protein generation, we encounter the following challenges:

- **Benchmarking** - While the field of molecule generation is well-documented with standardized benchmarking procedures, *generative* tasks in protein design are not as well-established, making it hard to objectively evaluate the quality of designed proteins.
- **Performance** - As the tasks in protein generation are generally more difficult than those in molecule generation, SOTA models still have room for improvement in several key areas like fold classification, gene ontology, and antibody CDR H3 generation.

While our paper focuses on generative models and applications, it is important to note that many current tasks are evaluated with predictive models, such as the affinity optimization task in antibody generation or the conditional generation task for molecules. In these cases, classifier networks are used to predict binding affinity or molecular properties, and improvements to these classification methods would naturally lead to more precise alignment with real-world biological applications.

Conclusion

The survey has provided an overview of the current landscape of generative AI in *de novo* drug design, focusing on molecule and protein generation. It has discussed important advancements in these fields, detailing the key datasets, model architectures, and evaluation metrics used. The paper also highlights key challenges and future directions, including improvements to benchmarking methods, improving explainability, and further alignment with real-world tasks to increase applicability. Overall, generative AI has shown great promise in the field of drug design, and continued research in this field can lead to exciting advancements in the future.

References

- Jurgen Drews. Drug discovery: a historical perspective. *science*, 287(5460):1960–1964, 2000.
- Soma Mandal, Sanat K Mandal, et al. Rational drug design. *European journal of pharmacology*, 625(1-3):90–100, 2009.
- Lucy J Colwell. Statistical and machine learning approaches to predicting protein–ligand interactions. *Current opinion in structural biology*, 49:123–128, 2018.
- Christopher Horvath. Comparison of preclinical development programs for small molecules (drugs/pharmaceuticals) and large molecules (biologics/biopharmaceuticals): studies, timing, materials, and costs. *Pharmaceutical Sciences Encyclopedia: Drug Discovery, Development, and Manufacturing*, pages 1–35, 2010.
- Gregory Sliwoski, Sandeepkumar Kothiwale, Jens Meiler, and Edward W Lowe. Computational methods in drug discovery. *Pharmacological reviews*, 66(1):334–395, 2014.
- Petra Schneider, W Patrick Walters, Alleyn T Plowright, Norman Sieroka, Jennifer Listgarten, Robert A Goodnow Jr, Jasmin Fisher, Johanna M Jansen, José S Duca, Thomas S Rush, et al. Rethinking drug design in the artificial intelligence era. *Nature Reviews Drug Discovery*, 19(5):353–364, 2020.
- Yankang Jing, Yuemin Bian, Ziheng Hu, Lirong Wang, and Xiang-Qun Sean Xie. Deep learning for drug design: an artificial intelligence paradigm for drug discovery in the big data era. *The AAPS journal*, 20:1–10, 2018.
- Pavel Polishchuk. Interpretation of quantitative structure–activity relationship models: past, present, and future. *Journal of Chemical Information and Modeling*, 57(11):2618–2639, 2017.
- Chartchalerm Isarankura-Na-Ayudhya, Thanakorn Naenna, Chanin Nantasenam, and Virapong Prachayasittikul. A practical overview of quantitative structure–activity relationship. 2009.
- Zheng Li, Siwen Wang, Wei Shan Chin, Luke E Achenie, and Hongliang Xin. High-throughput screening of bimetallic catalysts enabled by machine learning. *Journal of Materials Chemistry A*, 5(46):24131–24138, 2017.
- Hongjian Li, Kam-Heung Sze, Gang Lu, and Pedro J Ballester. Machine-learning scoring functions for structure-based virtual screening. *Wiley Interdisciplinary Reviews: Computational Molecular Science*, 11(1):e1478, 2021.
- Kevin K Yang, Zachary Wu, and Frances H Arnold. Machine-learning-guided directed evolution for protein engineering. *Nature methods*, 16(8):687–694, 2019.
- Zachary Wu, SB Jennifer Kan, Russell D Lewis, Bruce J Wittmann, and Frances H Arnold. Machine learning-assisted directed protein evolution with combinatorial libraries. *Proceedings of the National Academy of Sciences*, 116(18):8852–8858, 2019.
- Markus Hartenfeller and Gisbert Schneider. De novo drug design. *Chemoinformatics and computational chemical biology*, pages 299–323, 2011.
- Varnavas D Mouchlis, Antreas Afantitis, Angela Serra, Michele Fratello, Anastasios G Papadiamantis, Vassilis Aidinis, Iseult Lynch, Dario Greco, and Georgia Melagraki. Advances in de novo drug design: from conventional to machine learning methods. *International journal of molecular sciences*, 22(4):1676, 2021.
- Angelica Nakagawa Lima, Eric Allison Philot, Gustavo Henrique Goulart Trossini, Luis Paulo Barbour Scott, Vinícius Gonçalves Maltarollo, and Kathia Maria Honorio. Use of machine learning approaches for novel drug discovery. *Expert opinion on drug discovery*, 11(3):225–239, 2016.
- Meiqiu Dong, Xinrui Miao, Romain Brisse, Wenli Deng, Bruno Joussetme, and Fabien Silly. Molecular trapping in two-dimensional chiral organic kagomé nanoarchitectures composed of baravelle spiral triangle enantiomers. *NPG Asia Materials*, 12(1):20, 2020.
- Lilian Weng. What are diffusion models?, Jul 2021.
- Jagadeesan Ganapathy, Kannan Damodharan, Bakthadoss Manickam, and Aravindhan Sanmargam. Crystal and molecular structure of 4, 6-dimethyl-9-phenyl-8, 12-dioxo-4, 6-diazatetracyclo [8.8.0.0.2, 7.0.13, 18] octadeca-2 (7), 13, 15, 17-tetraene-3, 5, 11-trione 2-ethoxyphenyl (2e)-but-2-enoate. *Journal of the Chosun Natural Science*, 6(4):197–204, 2013.
- Thalles Santos Silva. A few words on representation learning, Apr 2021.
- Protein structure prediction.
- Embl-Ebi. Levels of protein structure – quaternary.
- Jun Zhao, Ruth Nussinov, Wen-Jin Wu, and Buyong Ma. In silico methods in antibody design. *Antibodies*, 7(3):22, 2018.
- Mingyang Wang, Zhe Wang, Huiyong Sun, Jike Wang, Chao Shen, Gaoqi Weng, Xin Chai, Honglin Li, Dongsheng Cao, and Tingjun Hou. Deep learning approaches for de novo drug design: An overview. *Current Opinion in Structural Biology*, 72:135–144, 2022.
- Peter S Kutchukian and Eugene I Shakhnovich. De novo design: balancing novelty and confined chemical space. *Expert opinion on drug discovery*, 5(8):789–812, 2010.
- Xuhan Liu, Adriaan P IJzerman, and Gerard JP van Westen. Computational approaches for de novo drug design: past, present, and future. *Artificial neural networks*, pages 139–165, 2020.
- Joseph A DiMasi, Henry G Grabowski, and Ronald W Hansen. The cost of drug development. *New England Journal of Medicine*, 372(20):1972–1972, 2015.
- Shaun M Lippow and Bruce Tidor. Progress in computational protein design. *Current opinion in biotechnology*, 18(4):305–311, 2007.
- Wei Zhou, Yonghua Wang, Aiping Lu, and Ge Zhang. Systems pharmacology in small molecular drug discovery. *International journal of molecular sciences*, 17(2):246, 2016.
- G Richard Bickerton, Gaia V Paolini, Jérémy Besnard, Sorel Muresan, and Andrew L Hopkins. Quantifying the chemical beauty of drugs. *Nature chemistry*, 4(2):90–98, 2012.
- Oleg Ursu, Anwar Rayan, Amiram Goldblum, and Tudor I Oprea. Understanding drug-likeness. *Wiley Interdisciplinary Reviews: Computational Molecular Science*, 1(5):760–781, 2011.
- Pavel G Polishchuk, Timur I Madzhidov, and Alexandre Varnek. Estimation of the size of drug-like chemical space based on gdb-17 data. *Journal of computer-aided molecular design*, 27:675–679, 2013.
- Joseph A DiMasi, Henry G Grabowski, and Ronald W Hansen. Innovation in the pharmaceutical industry: new estimates of r&d costs. *Journal of health economics*, 47:20–33, 2016.

34. Madura KP Jayatunga, Wen Xie, Ludwig Ruder, Ulrik Schulze, and Christoph Meier. Ai in small-molecule drug discovery: A coming wave. *Nat. Rev. Drug Discov*, 21:175–176, 2022.
35. Wenze Ding, Kenta Nakai, and Haipeng Gong. Protein design via deep learning. *Briefings in bioinformatics*, 23(3):bbac102, 2022.
36. Wenhao Gao, Sai Pooja Mahajan, Jeremias Sulam, and Jeffrey J Gray. Deep learning in protein structural modeling and design. *Patterns*, 1(9), 2020.
37. Po-Ssu Huang, Scott E Boyken, and David Baker. The coming of age of de novo protein design. *Nature*, 537(7620):320–327, 2016.
38. Ningyu Zhang, Zhen Bi, Xiaozhuan Liang, Siyuan Cheng, Haosen Hong, Shumin Deng, Jiazhang Lian, Qiang Zhang, and HuaJun Chen. Ontoprotein: Protein pretraining with gene ontology embedding. *arXiv preprint arXiv:2201.11147*, 2022.
39. Hong-Yu Zhou, Yunxiang Fu, Zhicheng Zhang, Cheng Bian, and Yizhou Yu. Protein representation learning via knowledge enhanced primary structure modeling. *bioRxiv*, pages 2023–01, 2023.
40. Chang Ma, Haiteng Zhao, Lin Zheng, Jiayi Xin, Qintong Li, Lijun Wu, Zhihong Deng, Yang Lu, Qi Liu, and Lingpeng Kong. Retrieved sequence augmentation for protein representation learning. *bioRxiv*, pages 2023–02, 2023.
41. Philip A Romero and Frances H Arnold. Exploring protein fitness landscapes by directed evolution. *Nature reviews Molecular cell biology*, 10(12):866–876, 2009.
42. Bassil I Dahiyat and Stephen L Mayo. De novo protein design: fully automated sequence selection. *Science*, 278(5335):82–87, 1997.
43. Zaixi Zhang, Jiaxian Yan, Qi Liu, and Enhong Che. A systematic survey in geometric deep learning for structure-based drug design. *arXiv preprint arXiv:2306.11768*, 2023.
44. Morgan Thomas, Andreas Bender, and Chris de Graaf. Integrating structure-based approaches in generative molecular design. *Current Opinion in Structural Biology*, 79:102559, 2023.
45. Rahmad Akbar, Habib Bashour, Puneet Rawat, Philippe A Robert, Eva Smorodina, Tudor-Stefan Cotet, Karine Flem-Karlsen, Robert Frank, Brij Bhushan Mehta, Mai Ha Vu, et al. Progress and challenges for the machine learning-based design of fit-for-purpose monoclonal antibodies. In *MAbs*, volume 14, page 2008790. Taylor & Francis, 2022.
46. Alissa M Hummer, Brennan Abanades, and Charlotte M Deane. Advances in computational structure-based antibody design. *Current Opinion in Structural Biology*, 74:102379, 2022.
47. Michael Chungyoun and Jeffrey J Gray. Ai models for protein design are driving antibody engineering. *Current Opinion in Biomedical Engineering*, page 100473, 2023.
48. Jisun Kim, Matthew McFee, Qiao Fang, Osama Abdin, and Philip M Kim. Computational and artificial intelligence-based methods for antibody development. *Trends in Pharmacological Sciences*, 2023.
49. Mengchun Zhang, Maryam Qamar, Taegoo Kang, Yuna Jung, Chenshuang Zhang, Sung-Ho Bae, and Chaoning Zhang. A survey on graph diffusion models: Generative ai in science for molecule, protein and material. *arXiv preprint arXiv:2304.01565*, 2023.
50. Zhiye Guo, Jian Liu, Yanli Wang, Mengrui Chen, Duolin Wang, Dong Xu, and Jianlin Cheng. Diffusion models in bioinformatics: A new wave of deep learning revolution in action. *arXiv preprint arXiv:2302.10907*, 2023.
51. Ian Goodfellow, Jean Pouget-Abadie, Mehdi Mirza, Bing Xu, David Warde-Farley, Sherjil Ozair, Aaron Courville, and Yoshua Bengio. Generative adversarial nets. *Advances in neural information processing systems*, 27, 2014.
52. Diederik P Kingma and Max Welling. Auto-encoding variational bayes. *arXiv preprint arXiv:1312.6114*, 2013.
53. Danilo Rezende and Shakir Mohamed. Variational inference with normalizing flows. In *International conference on machine learning*, pages 1530–1538. PMLR, 2015.
54. Ling Yang, Zhilong Zhang, Yang Song, Shenda Hong, Runsheng Xu, Yue Zhao, Yingxia Shao, Wentao Zhang, Bin Cui, and Ming-Hsuan Yang. Diffusion models: A comprehensive survey of methods and applications. *arXiv preprint arXiv:2209.00796*, 2022.
55. Tim Van Erven and Peter Harremo. Rényi divergence and kullback-leibler divergence. *IEEE Transactions on Information Theory*, 60(7):3797–3820, 2014.
56. Jonathan Ho, Ajay Jain, and Pieter Abbeel. Denoising diffusion probabilistic models. *Advances in neural information processing systems*, 33:6840–6851, 2020.
57. Yang Song and Stefano Ermon. Generative modeling by estimating gradients of the data distribution. *Advances in neural information processing systems*, 32, 2019.
58. Yang Song, Jascha Sohl-Dickstein, Diederik P Kingma, Abhishek Kumar, Stefano Ermon, and Ben Poole. Score-based generative modeling through stochastic differential equations. *arXiv preprint arXiv:2011.13456*, 2020.
59. Nobuyuki Ikeda, Sinzo Watanabe, Masatoshi Fukushima, and Hiroshi Kunita. *Itô’s stochastic calculus and probability theory*. Springer Science & Business Media, 2012.
60. Jacob Austin, Daniel D Johnson, Jonathan Ho, Daniel Tarlow, and Rianne Van Den Berg. Structured denoising diffusion models in discrete state-spaces. *Advances in Neural Information Processing Systems*, 34:17981–17993, 2021.
61. Franco Scarselli, Marco Gori, Ah Chung Tsoi, Markus Hagenbuchner, and Gabriele Monfardini. The graph neural network model. *IEEE transactions on neural networks*, 20(1):61–80, 2008.
62. Victor Garcia Satorras, Emiel Hoogeboom, and Max Welling. E (n) equivariant graph neural networks. In *International conference on machine learning*, pages 9323–9332. PMLR, 2021.
63. Ashish Vaswani, Noam Shazeer, Niki Parmar, Jakob Uszkoreit, Llion Jones, Aidan N Gomez, Lukasz Kaiser, and Illia Polosukhin. Attention is all you need. *Advances in neural information processing systems*, 30, 2017.
64. Marius-Constantin Popescu, Valentina E Balas, Liliana Perescu-Popescu, and Nikos Mastorakis. Multilayer perceptron and neural networks. *WSEAS Transactions on Circuits and Systems*, 8(7):579–588, 2009.
65. Yann LeCun, Sumit Chopra, Raia Hadsell, M Ranzato, and Fugie Huang. A tutorial on energy-based learning. *Predicting structured data*, 1(0), 2006.
66. Jiquan Ngiam, Zhenghao Chen, Pang W Koh, and Andrew Y Ng. Learning deep energy models. In *Proceedings of the 28th international conference on machine learning (ICML-11)*, pages 1105–1112, 2011.

67. Kristof Schütt, Pieter-Jan Kindermans, Huziel Enoc Saucedo Felix, Stefan Chmiela, Alexandre Tkatchenko, and Klaus-Robert Müller. Schnet: A continuous-filter convolutional neural network for modeling quantum interactions. *Advances in neural information processing systems*, 30, 2017.
68. Sepp Hochreiter and Jürgen Schmidhuber. Long short-term memory. *Neural computation*, 9(8):1735–1780, 1997.
69. Jacob Devlin, Ming-Wei Chang, Kenton Lee, and Kristina Toutanova. Bert: Pre-training of deep bidirectional transformers for language understanding. *arXiv preprint arXiv:1810.04805*, 2018.
70. Justin Gilmer, Samuel S Schoenholz, Patrick F Riley, Oriol Vinyals, and George E Dahl. Neural message passing for quantum chemistry. In *International conference on machine learning*, pages 1263–1272. PMLR, 2017.
71. Thomas N Kipf and Max Welling. Semi-supervised classification with graph convolutional networks. *arXiv preprint arXiv:1609.02907*, 2016.
72. Keyulu Xu, Weihua Hu, Jure Leskovec, and Stefanie Jegelka. How powerful are graph neural networks? *arXiv preprint arXiv:1810.00826*, 2018.
73. Yann LeCun, Bernhard Boser, John S Denker, Donnie Henderson, Richard E Howard, Wayne Hubbard, and Lawrence D Jackel. Backpropagation applied to handwritten zip code recognition. *Neural computation*, 1(4):541–551, 1989.
74. Jiuxiang Gu, Zhenhua Wang, Jason Kuen, Lianyang Ma, Amir Shahroudy, Bing Shuai, Ting Liu, Xingxing Wang, Gang Wang, Jianfei Cai, et al. Recent advances in convolutional neural networks. *Pattern recognition*, 77:354–377, 2018.
75. Keiron O’Shea and Ryan Nash. An introduction to convolutional neural networks. *arXiv preprint arXiv:1511.08458*, 2015.
76. Xiangru Tang, Andrew Tran, Jeffrey Tan, and Mark B Gerstein. Mollm: A unified language model for integrating biomedical text with 2d and 3d molecular representations. *bioRxiv*, pages 2023–11, 2023.
77. Raghunathan Ramakrishnan, Pavlo O Dral, Matthias Rupp, and O Anatole Von Lilienfeld. Quantum chemistry structures and properties of 134 kilo molecules. *Scientific data*, 1(1):1–7, 2014.
78. Simon Axelrod and Rafael Gomez-Bombarelli. Geom, energy-annotated molecular conformations for property prediction and molecular generation. *Scientific Data*, 9(1):185, 2022.
79. Clement Vignac and Pascal Frossard. Top-n: Equivariant set and graph generation without exchangeability. *arXiv preprint arXiv:2110.02096*, 2021.
80. Niklas Gebauer, Michael Gastegger, and Kristof Schütt. Symmetry-adapted generation of 3d point sets for the targeted discovery of molecules. *Advances in neural information processing systems*, 32, 2019.
81. Minkai Xu, Alexander Powers, Ron Dror, Stefano Ermon, and Jure Leskovec. Geometric latent diffusion models for 3d molecule generation. *arXiv preprint arXiv:2305.01140*, 2023.
82. Victor Garcia Satorras, Emiel Hoogeboom, Fabian Fuchs, Ingmar Posner, and Max Welling. E (n) equivariant normalizing flows. *Advances in Neural Information Processing Systems*, 34:4181–4192, 2021.
83. Alex Morehead and Jianlin Cheng. Geometry-complete diffusion for 3d molecule generation. *arXiv preprint arXiv:2302.04313*, 2023.
84. Lei Huang, Hengtong Zhang, Tingyang Xu, and Ka-Chun Wong. Mdm: Molecular diffusion model for 3d molecule generation. *arXiv preprint arXiv:2209.05710*, 2022.
85. Han Huang, Leilei Sun, Bowen Du, and Weifeng Lv. Learning joint 2d & 3d diffusion models for complete molecule generation. *arXiv preprint arXiv:2305.12347*, 2023.
86. Clement Vignac, Nagham Osman, Laura Toni, and Pascal Frossard. Midi: Mixed graph and 3d denoising diffusion for molecule generation. *arXiv preprint arXiv:2302.09048*, 2023.
87. Rafael Gómez-Bombarelli, Jennifer N Wei, David Duvenaud, José Miguel Hernández-Lobato, Benjamín Sánchez-Lengeling, Dennis Sheberla, Jorge Aguilera-Iparraguirre, Timothy D Hirzel, Ryan P Adams, and Alán Aspuru-Guzik. Automatic chemical design using a data-driven continuous representation of molecules. *ACS central science*, 4(2):268–276, 2018.
88. Matt J Kusner, Brooks Paige, and José Miguel Hernández-Lobato. Grammar variational autoencoder. In *International conference on machine learning*, pages 1945–1954. PMLR, 2017.
89. Hanjun Dai, Yingtao Tian, Bo Dai, Steven Skiena, and Le Song. Syntax-directed variational autoencoder for structured data. *arXiv preprint arXiv:1802.08786*, 2018.
90. Wengong Jin, Regina Barzilay, and Tommi Jaakkola. Junction tree variational autoencoder for molecular graph generation. In *International conference on machine learning*, pages 2323–2332. PMLR, 2018.
91. Emiel Hoogeboom, Victor Garcia Satorras, Clément Vignac, and Max Welling. Equivariant diffusion for molecule generation in 3d. In *International Conference on Machine Learning*, pages 8867–8887. PMLR, 2022.
92. Paul G. Francoeur, Tomohide Masuda, Jocelyn Sunseri, Andrew Jia, Richard B. Iovanisci, Ian Snyder, and David R. Koes. Three-dimensional convolutional neural networks and a cross-docked data set for structure-based drug design. *Journal of Chemical Information and Modeling*, 60(9):4200–4215, 2020. PMID: 32865404.
93. Liegi Hu, Mark L Benson, Richard D Smith, Michael G Lerner, and Heather A Carlson. Binding moad (mother of all databases). *Proteins: Structure, Function, and Bioinformatics*, 60(3):333–340, 2005.
94. John J. Irwin, Khanh G. Tang, Jennifer Young, Chinzorig Dandarchuluun, Benjamin R. Wong, Munkhzul Khurelbaatar, Yurii S. Moroz, John Mayfield, and Roger A. Sayle. Zinc20—a free ultralarge-scale chemical database for ligand discovery. *Journal of Chemical Information and Modeling*, 60(12):6065–6073, 2020. PMID: 33118813.
95. Helen M Berman, John Westbrook, Zukang Feng, Gary Gilliland, Talapady N Bhat, Helge Weissig, Ilya N Shindyalov, and Philip E Bourne. The protein data bank. *Nucleic acids research*, 28(1):235–242, 2000.
96. Oleg Trott and Arthur J. Olson. Autodock vina: Improving the speed and accuracy of docking with a new scoring function, efficient optimization, and multithreading. *Journal of Computational Chemistry*, 31(2):455–461, 2010.
97. Peter Ertl and Ansgar Schuffenhauer. Estimation of synthetic accessibility score of drug-like molecules based on molecular complexity and fragment contributions. *Journal of cheminformatics*, 1:1–11, 2009.

98. Taffee T Tanimoto. Elementary mathematical theory of classification and prediction. 1958.
99. Yuesen Li, Chengyi Gao, Xin Song, Xiangyu Wang, Yungang Xu, and Suxia Han. Druggpt: A gpt-based strategy for designing potential ligands targeting specific proteins. *bioRxiv*, 2023.
100. Tomohide Masuda, Matthew Ragoza, and David Ryan Koes. Generating 3d molecular structures conditional on a receptor binding site with deep generative models. *arXiv preprint arXiv:2010.14442*, 2020.
101. Xingang Peng, Shitong Luo, Jiaqi Guan, Qi Xie, Jian Peng, and Jianzhu Ma. Pocket2mol: Efficient molecular sampling based on 3d protein pockets. In *International Conference on Machine Learning*, pages 17644–17655. PMLR, 2022.
102. Shitong Luo, Jiaqi Guan, Jianzhu Ma, and Jian Peng. A 3d generative model for structure-based drug design. *Advances in Neural Information Processing Systems*, 34:6229–6239, 2021.
103. Jiaqi Guan, Wesley Wei Qian, Xingang Peng, Yufeng Su, Jian Peng, and Jianzhu Ma. 3d equivariant diffusion for target-aware molecule generation and affinity prediction. *arXiv preprint arXiv:2303.03543*, 2023.
104. Arne Schneuing, Yuanqi Du, Charles Harris, Arian Jamasb, Ilia Igashov, Weitao Du, Tom Blundell, Pietro Lió, Carla Gomes, Max Welling, et al. Structure-based drug design with equivariant diffusion models. *arXiv preprint arXiv:2210.13695*, 2022.
105. Minkai Xu, Shitong Luo, Yoshua Bengio, Jian Peng, and Jian Tang. Learning neural generative dynamics for molecular conformation generation. *arXiv preprint arXiv:2102.10240*, 2021.
106. Elman Mansimov, Omar Mahmood, Seokho Kang, and Kyunghyun Cho. Molecular geometry prediction using a deep generative graph neural network. *Scientific reports*, 9(1):20381, 2019.
107. Gregor NC Simm and José Miguel Hernández-Lobato. A generative model for molecular distance geometry. *arXiv preprint arXiv:1909.11459*, 2019.
108. Octavian Ganea, Lagnajit Pattanaik, Connor Coley, Regina Barzilay, Klavs Jensen, William Green, and Tommi Jaakkola. Geomol: Torsional geometric generation of molecular 3d conformer ensembles. *Advances in Neural Information Processing Systems*, 34:13757–13769, 2021.
109. Chence Shi, Shitong Luo, Minkai Xu, and Jian Tang. Learning gradient fields for molecular conformation generation. In *International conference on machine learning*, pages 9558–9568. PMLR, 2021.
110. Weihua Hu, Muhammed Shuaibi, Abhishek Das, Siddharth Goyal, Anuroop Sriram, Jure Leskovec, Devi Parikh, and C Lawrence Zitnick. Forcenet: A graph neural network for large-scale quantum calculations. *arXiv preprint arXiv:2103.01436*, 2021.
111. Shitong Luo, Chence Shi, Minkai Xu, and Jian Tang. Predicting molecular conformation via dynamic graph score matching. *Advances in Neural Information Processing Systems*, 34:19784–19795, 2021.
112. Minkai Xu, Lantao Yu, Yang Song, Chence Shi, Stefano Ermon, and Jian Tang. Geodiff: A geometric diffusion model for molecular conformation generation. *arXiv preprint arXiv:2203.02923*, 2022.
113. Bowen Jing, Gabriele Corso, Jeffrey Chang, Regina Barzilay, and Tommi Jaakkola. Torsional diffusion for molecular conformer generation. *arXiv preprint arXiv:2206.01729*, 2022.
114. Michael J Lopez and Shamim S Mohiuddin. Biochemistry, essential amino acids. 2020.
115. Areski Flissi, Emma Ricart, Clémentine Campart, Mickael Chevalier, Yoann Dufresne, Juraj Michalik, Philippe Jacques, Christophe Flahaut, Frederique Lisacek, Valérie Leclère, et al. Norine: Update of the nonribosomal peptide resource. *Nucleic acids research*, 48(D1):D465–D469, 2020.
116. Ahmed Elnaggar, Michael Heinzinger, Christian Dallago, Ghalia Rehawi, Yu Wang, Llion Jones, Tom Gibbs, Tamas Feher, Christoph Angerer, Martin Steinegger, et al. Prottrans: Toward understanding the language of life through self-supervised learning. *IEEE transactions on pattern analysis and machine intelligence*, 44(10):7112–7127, 2021.
117. Alexander Rives, Joshua Meier, Tom Sercu, Siddharth Goyal, Zeming Lin, Jason Liu, Demi Guo, Myle Ott, C Lawrence Zitnick, Jerry Ma, et al. Biological structure and function emerge from scaling unsupervised learning to 250 million protein sequences. *Proceedings of the National Academy of Sciences*, 118(15):e2016239118, 2021.
118. Suyue Lyu, Shahin Sowlati-Hashjin, and Michael Garton. Proteinvae: Variational autoencoder for translational protein design. *bioRxiv*, pages 2023–03, 2023.
119. Zeming Lin, Halil Akin, Roshan Rao, Brian Hie, Zhongkai Zhu, Wenting Lu, Nikita Smetanin, Robert Verkuil, Ori Kabeli, Yaniv Shmueli, Allan dos Santos Costa, Maryam Fazel-Zarandi, Tom Sercu, Salvatore Candido, and Alexander Rives. Evolutionary-scale prediction of atomic-level protein structure with a language model. *Science*, 379(6637):1123–1130, 2023.
120. Jeffrey A Ruffolo, Jeffrey J Gray, and Jeremias Sulam. Deciphering antibody affinity maturation with language models and weakly supervised learning. *arXiv preprint arXiv:2112.07782*, 2021.
121. Xiangrui Gao, Lipeng Lai, and Changling Cao. Pre-training with a rational approach for antibody. *bioRxiv*, pages 2023–01, 2023.
122. Jinwoo Leem, Laura S Mitchell, James HR Farmery, Justin Barton, and Jacob D Galson. Deciphering the language of antibodies using self-supervised learning. *Patterns*, 3(7):100513, 2022.
123. Pengcheng He, Xiaodong Liu, Jianfeng Gao, and Weizhu Chen. Deberta: Decoding-enhanced bert with disentangled attention. *arXiv preprint arXiv:2006.03654*, 2020.
124. Yinhan Liu, Myle Ott, Naman Goyal, Jingfei Du, Mandar Joshi, Danqi Chen, Omer Levy, Mike Lewis, Luke Zettlemoyer, and Veselin Stoyanov. Roberta: A robustly optimized bert pretraining approach. *arXiv preprint arXiv:1907.11692*, 2019.
125. Andriy Kryshchak, Torsten Schwede, Maya Topf, Krzysztof Fidelis, and John Moulton. Critical assessment of methods of protein structure prediction (casp)—round xiv. *Proteins: Structure, Function, and Bioinformatics*, 89(12):1607–1617, 2021.
126. Jürgen Haas, Alessandro Barbato, Dario Behringer, Gabriel Studer, Steven Roth, Martino Bertoni, Khaled Mostaguir, Rafal Gumienny, and Torsten Schwede. Continuous automated model evaluation (cameo) complementing the critical assessment of structure prediction in casp12. *Proteins: Structure, Function, and Bioinformatics*, 86:387–398, 2018.

127. Adam Zemla. Lga: a method for finding 3d similarities in protein structures. *Nucleic acids research*, 31(13):3370–3374, 2003.
128. Yang Zhang and Jeffrey Skolnick. Scoring function for automated assessment of protein structure template quality. *Proteins: Structure, Function, and Bioinformatics*, 57(4):702–710, 2004.
129. Valerio Mariani, Marco Biasini, Alessandro Barbato, and Torsten Schwede. Iddt: a local superposition-free score for comparing protein structures and models using distance difference tests. *Bioinformatics*, 29(21):2722–2728, 2013.
130. John Jumper, Richard Evans, Alexander Pritzel, Tim Green, Michael Figurnov, Olaf Ronneberger, Kathryn Tunyasuvunakool, Russ Bates, Augustin Žídek, Anna Potapenko, et al. Highly accurate protein structure prediction with alphafold. *Nature*, 596(7873):583–589, 2021.
131. Bowen Jing, Ezra Erives, Peter Pao-Huang, Gabriele Corso, Bonnie Berger, and Tommi Jaakkola. Eigenfold: Generative protein structure prediction with diffusion models. *arXiv preprint arXiv:2304.02198*, 2023.
132. Minkyung Baek, Frank DiMaio, Ivan Anishchenko, Justas Dauparas, Sergey Ovchinnikov, Gyu Rie Lee, Jue Wang, Qian Cong, Lisa N. Kinch, R. Dustin Schaeffer, Claudia Millán, Hahnbeom Park, Carson Adams, Caleb R. Glassman, Andy DeGiovanni, Jose H. Pereira, Andria V. Rodrigues, Alberdina A. van Dijk, Ana C. Ebrecht, Diederik J. Opperman, Theo Sagmeister, Christoph Buhlheller, Tea Pavkov-Keller, Manoj K. Rathinaswamy, Udit Dalwadi, Calvin K. Yip, John E. Burke, K. Christopher Garcia, Nick V. Grishin, Paul D. Adams, Randy J. Read, and David Baker. Accurate prediction of protein structures and interactions using a three-track neural network. *Science*, 373(6557):871–876, 2021.
133. Zongyang Du, Hong Su, Wenkai Wang, Lisha Ye, Hong Wei, Zhenling Peng, Ivan Anishchenko, David Baker, and Jianyi Yang. The trRosetta server for fast and accurate protein structure prediction. *Nature News*, Nov 2021.
134. Jeffrey A Ruffolo, Lee-Shin Chu, Sai Pooja Mahajan, and Jeffrey J Gray. Fast, accurate antibody structure prediction from deep learning on massive set of natural antibodies. *Nature communications*, 14(1):2389, 2023.
135. Jiayang Wu, Fandi Wu, Biaobin Jiang, Wei Liu, and Peilin Zhao. tfold-ab: Fast and accurate antibody structure prediction without sequence homologs. *bioRxiv*, pages 2022–11, 2022.
136. Mihaly Varadi, Stephen Anyango, Mandar Deshpande, Sreenath Nair, Cindy Natassia, Galabina Yordanova, David Yuan, Oana Stroe, Gemma Wood, Agata Laydon, et al. Alphafold protein structure database: massively expanding the structural coverage of protein-sequence space with high-accuracy models. *Nucleic acids research*, 50(D1):D439–D444, 2022.
137. Alexey G Murzin, Steven E Brenner, Tim Hubbard, and Cyrus Chothia. Scop: a structural classification of proteins database for the investigation of sequences and structures. *Journal of molecular biology*, 247(4):536–540, 1995.
138. John-Marc Chandonia, Lindsey Guan, Shiangyi Lin, Changhua Yu, Naomi K Fox, and Steven E Brenner. Scope: improvements to the structural classification of proteins—extended database to facilitate variant interpretation and machine learning. *Nucleic acids research*, 50(D1):D553–D559, 2022.
139. Ian Sillitoe, Tony E Lewis, Alison Cuff, Sayoni Das, Paul Ashford, Natalie L Dawson, Nicholas Furnham, Roman A Laskowski, David Lee, Jonathan G Lees, et al. Cath: comprehensive structural and functional annotations for genome sequences. *Nucleic acids research*, 43(D1):D376–D381, 2015.
- 140.
141. Brian L Trippe, Jason Yim, Doug Tischer, David Baker, Tamara Broderick, Regina Barzilay, and Tommi Jaakkola. Diffusion probabilistic modeling of protein backbones in 3d for the motif-scaffolding problem. *arXiv preprint arXiv:2206.04119*, 2022.
142. Justas Dauparas, Ivan Anishchenko, Nathaniel Bennett, Hua Bai, Robert J Ragotte, Lukas F Milles, Basile IM Wicky, Alexis Courbet, Rob J de Haas, Neville Bethel, et al. Robust deep learning–based protein sequence design using proteinmpnn. *Science*, 378(6615):49–56, 2022.
143. Cong Fu, Keqiang Yan, Limei Wang, Wing Yee Au, Michael McThrow, Tao Komikado, Koji Maruhashi, Kanji Uchino, Xiaoning Qian, and Shuiwang Ji. A latent diffusion model for protein structure generation. *arXiv preprint arXiv:2305.04120*, 2023.
144. Kevin E Wu, Kevin K Yang, Rianne van den Berg, James Y Zou, Alex X Lu, and Ava P Amini. Protein structure generation via folding diffusion. *arXiv preprint arXiv:2209.15611*, 2022.
145. Jason Yim, Brian L Trippe, Valentin De Bortoli, Emile Mathieu, Arnaud Doucet, Regina Barzilay, and Tommi Jaakkola. Se (3) diffusion model with application to protein backbone generation. *arXiv preprint arXiv:2302.02277*, 2023.
146. Yeqing Lin and Mohammed AlQuraishi. Generating novel, designable, and diverse protein structures by equivariantly diffusing oriented residue clouds. *arXiv preprint arXiv:2301.12485*, 2023.
147. Joseph L Watson, David Juergens, Nathaniel R Bennett, Brian L Trippe, Jason Yim, Helen E Eisenach, Woody Ahern, Andrew J Borst, Robert J Ragotte, Lukas F Milles, et al. De novo design of protein structure and function with rfdiffusion. *Nature*, 620(7976):1089–1100, 2023.
148. Zhenqiao Song, Yunlong Zhao, Yufei Song, Wenxian Shi, Yang Yang, and Lei Li. Joint design of protein sequence and structure based on motifs. *arXiv preprint arXiv:2310.02546*, 2023.
149. Chence Shi, Chuanrui Wang, Jiarui Lu, Bozitao Zhong, and Jian Tang. Protein sequence and structure co-design with equivariant translation. *arXiv preprint arXiv:2210.08761*, 2022.
150. Alexander E Chu, Lucy Cheng, Gina El Nesr, Minkai Xu, and Po-Ssu Huang. An all-atom protein generative model. *bioRxiv*, pages 2023–05, 2023.
151. Bowen Jing, Stephan Eismann, Patricia Suriana, Raphael JL Townshend, and Ron Dror. Learning from protein structure with geometric vector perceptrons. *arXiv preprint arXiv:2009.01411*, 2020.
152. Emre Sevgen, Joshua Moller, Adrian Lange, John Parker, Sean Quigley, Jeff Mayer, Poonam Srivastava, Sitaram Gayatri, David Hosfield, Maria Korshunova, et al. Protvae: Protein transformer variational autoencoder for functional protein design. *bioRxiv*, pages 2023–01, 2023.
153. Bionemo.
154. Donatas Repecka, Vyktintas Jauniskis, Laurynas Karpus, Elzbieta Rembeza, Irmantas Rokaitis, Jan Zrimec, Simona Poviloniene, Audrius Laurynenas, Sandra Viknander,

- Wissam Abuajwa, et al. Expanding functional protein sequence spaces using generative adversarial networks. *Nature Machine Intelligence*, 3(4):324–333, 2021.
155. Alexander E Chu, Lucy Cheng, Gina El Nesr, Minkai Xu, and Po-Ssu Huang. An all-atom protein generative model. *bioRxiv*, pages 2023–05, 2023.
156. Namrata Anand and Tudor Achim. Protein structure and sequence generation with equivariant denoising diffusion probabilistic models. *arXiv preprint arXiv:2205.15019*, 2022.
157. Rahmad Akbar, Philippe A Robert, Cédric R Weber, Michael Widrich, Robert Frank, Milena Pavlović, Lonke Scheffer, Maria Chernigovskaya, Igor Snapkov, Andrei Slabodkin, et al. In silico proof of principle of machine learning-based antibody design at unconstrained scale. In *MAbs*, volume 14, page 2031482. Taylor & Francis, 2022.
158. Wengong Jin, Jeremy Wohlwend, Regina Barzilay, and Tommi Jaakkola. Iterative refinement graph neural network for antibody sequence-structure co-design. *arXiv preprint arXiv:2110.04624*, 2021.
159. Xiangzhe Kong, Wenbing Huang, and Yang Liu. End-to-end full-atom antibody design. *arXiv preprint arXiv:2302.00203*, 2023.
160. Rolf Apweiler, Amos Bairoch, Cathy H Wu, Winona C Barker, Brigitte Boeckmann, Serenella Ferro, Elisabeth Gasteiger, Hongzhan Huang, Rodrigo Lopez, Michele Magrane, et al. Uniprot: the universal protein knowledgebase. *Nucleic acids research*, 32(suppl_1):D115–D119, 2004.
161. Jaina Mistry, Sara Chuguransky, Lowri Williams, Matloob Qureshi, Gustavo A Salazar, Erik LL Sonnhammer, Silvio CE Tosatto, Lisanna Paladin, Shriya Raj, Lorna J Richardson, et al. Pfam: The protein families database in 2021. *Nucleic acids research*, 49(D1):D412–D419, 2021.
162. Roshan Rao, Nicholas Bhattacharya, Neil Thomas, Yan Duan, Peter Chen, John Canny, Pieter Abbeel, and Yun Song. Evaluating protein transfer learning with tape. *Advances in neural information processing systems*, 32, 2019.
163. Minghao Xu, Zuobai Zhang, Jiarui Lu, Zhaocheng Zhu, Yangtian Zhang, Ma Chang, Runcheng Liu, and Jian Tang. Peer: a comprehensive and multi-task benchmark for protein sequence understanding. *Advances in Neural Information Processing Systems*, 35:35156–35173, 2022.
164. John Moulton, Krzysztof Fidelis, Andriy Kryshchuk, Torsten Schwede, and Anna Tramontano. Critical assessment of methods of protein structure prediction (casp)—round xii. *Proteins: Structure, Function, and Bioinformatics*, 86:7–15, 2018.
165. R Dustin Schaeffer and Valerie Daggett. Protein folds and protein folding. *Protein Engineering, Design & Selection*, 24(1-2):11–19, 2011.
166. Jie Hou, Badri Adhikari, and Jianlin Cheng. DeepSF: deep convolutional neural network for mapping protein sequences to folds. *Bioinformatics*, 34(8):1295–1303, 2018.
167. Ethan C Alley, Grigory Khimulya, Surojit Biswas, Mohammed AlQuraishi, and George M Church. Unified rational protein engineering with sequence-based deep representation learning. *Nature methods*, 16(12):1315–1322, 2019.
168. Zuobai Zhang, Minghao Xu, Arian Jamasb, Vijil Chenthamarakshan, Aurelie Lozano, Payel Das, and Jian Tang. Protein representation learning by geometric structure pretraining. *arXiv preprint arXiv:2203.06125*, 2022.
169. Roshan M Rao, Jason Liu, Robert Verkuil, Joshua Meier, John Canny, Pieter Abbeel, Tom Sercu, and Alexander Rives. Msa transformer. In *International Conference on Machine Learning*, pages 8844–8856. PMLR, 2021.
170. Vladimir Gligorijević, P Douglas Renfrew, Tomasz Kosciolk, Julia Koehler Leman, Daniel Berenberg, Tommi Vatanen, Chris Chandler, Bryn C Taylor, Ian M Fisk, Hera Vlamakis, et al. Structure-based protein function prediction using graph convolutional networks. *Nature communications*, 12(1):3168, 2021.
171. Pedro Hermosilla, Marco Sch" afer, Matěj Lang, Gloria Fackelmann, Pere Pau Vázquez, Barbora Kozlíková, Michael Krone, Tobias Ritschel, and Timo Ropinski. Intrinsic-extrinsic convolution and pooling for learning on 3d protein structures. *arXiv preprint arXiv:2007.06252*, 2020.
172. Xiangzhe Kong, Wenbing Huang, and Yang Liu. Conditional antibody design as 3d equivariant graph translation. *arXiv preprint arXiv:2208.06073*, 2022.
173. Lin Li, Esther Gupta, John Spaeth, Leslie Shing, Tristan Bepler, and Rajmonda Sulo Caceres. Antibody representation learning for drug discovery. *arXiv preprint arXiv:2210.02881*, 2022.
174. Tobias H Olsen, Iain H Moal, and Charlotte M Deane. Ablang: an antibody language model for completing antibody sequences. *Bioinformatics Advances*, 2(1):vbac046, 2022.
175. Tobias H Olsen, Fergus Boyles, and Charlotte M Deane. Observed antibody space: A diverse database of cleaned, annotated, and translated unpaired and paired antibody sequences. *Protein Science*, 31(1):141–146, 2022.
176. Brennan Abanades, Guy Georges, Alexander Bujotzek, and Charlotte M Deane. Ablooper: fast accurate antibody cdr loop structure prediction with accuracy estimation. *Bioinformatics*, 38(7):1877–1880, 2022.
177. Brennan Abanades, Wing Ki Wong, Fergus Boyles, Guy Georges, Alexander Bujotzek, and Charlotte M Deane. Immunebuilder: Deep-learning models for predicting the structures of immune proteins. *Communications Biology*, 6(1):575, 2023.
178. James Dunbar, Konrad Krawczyk, Jinwoo Leem, Terry Baker, Angelika Fuchs, Guy Georges, Jiye Shi, and Charlotte M Deane. Sabdab: the structural antibody database. *Nucleic acids research*, 42(D1):D1140–D1146, 2014.
179. Jared Adolf-Bryfogle, Oleks Kalyuzhnyi, Michael Kubitz, Brian D Weitzner, Xiaozhen Hu, Yumiko Adachi, William R Schief, and Roland L Dunbrack Jr. Rosettaantibodydesign (rabd): A general framework for computational antibody design. *PLoS computational biology*, 14(4):e1006112, 2018.
180. Nicholas A Marze, Sergey Lyskov, and Jeffrey J Gray. Improved prediction of antibody vl–vh orientation. *Protein Engineering, Design and Selection*, 29(10):409–418, 2016.
181. Jeffrey A Ruffolo, Jeremias Sulam, and Jeffrey J Gray. Antibody structure prediction using interpretable deep learning. *Patterns*, 3(2):100406, 2022.
182. Yining Wang, Xumeng Gong, Shaochuan Li, Bing Yang, YiWu Sun, Chuan Shi, Hui Li, Yangang Wang, Cheng Yang, and Le Song. xtrimoabfold: Improving antibody structure prediction without multiple sequence

- alignments. *arXiv preprint arXiv:2212.00735*, 2022.
183. Jeffrey A Ruffolo, Carlos Guerra, Sai Pooja Mahajan, Jeremias Sulam, and Jeffrey J Gray. Geometric potentials from deep learning improve prediction of cdr h3 loop structures. *Bioinformatics*, 36(Supplement_1):i268–i275, 2020.
184. Natalia Zenkova, Ekaterina Sedykh, Tatiana Shugaeva, Vladislav Strashko, Timofei Ermak, and Aleksei Shpilman. Simple end-to-end deep learning model for cdr-h3 loop structure prediction. *arXiv preprint arXiv:2111.10656*, 2021.
185. Matthew McPartlon and Jinbo Xu. Deep learning for flexible and site-specific protein docking and design. *bioRxiv*, pages 2023–04, 2023.
186. Wengong Jin, Regina Barzilay, and Tommi Jaakkola. Antibody-antigen docking and design via hierarchical equivariant refinement. *arXiv preprint arXiv:2207.06616*, 2022.
187. Gennady Bocharov, Vitaly Volpert, Burkhard Ludewig, Andreas Meyerhans, Gennady Bocharov, Vitaly Volpert, Burkhard Ludewig, and Andreas Meyerhans. Basic principles of building a mathematical model of immune response. *Mathematical Immunology of Virus Infections*, pages 15–34, 2018.
188. F Stanzione, I Giangreco, and JC Cole. Chapter four—use of molecular docking computational tools in drug discovery. *Progress in Medicinal Chemistry*, pages 273–343.
189. Francesco Ambrosetti, Zuzana Jandova, and Alexandre MJJ Bonvin. A protocol for information-driven antibody-antigen modelling with the haddock2. 4 webserver. *arXiv preprint arXiv:2005.03283*, 2020.
190. Justina Jankauskaitė, Brian Jiménez-García, Justas Dapkūnas, Juan Fernández-Recio, and Iain H Moal. Skempi 2.0: an updated benchmark of changes in protein–protein binding energy, kinetics and thermodynamics upon mutation. *Bioinformatics*, 35(3):462–469, 2019.
191. Sisi Shan, Shitong Luo, Ziqing Yang, Junxian Hong, Yufeng Su, Fan Ding, Lili Fu, Chenyu Li, Peng Chen, Jianzhu Ma, et al. Deep learning guided optimization of human antibody against sars-cov-2 variants with broad neutralization. *Proceedings of the National Academy of Sciences*, 119(11):e2122954119, 2022.
192. Cheng Tan, Zhangyang Gao, and Stan Z Li. Protein complex invariant embedding with cross-gate mlp is a one-shot antibody designer. *arXiv preprint arXiv:2305.09480*, 2023.
193. Shitong Luo, Yufeng Su, Xingang Peng, Sheng Wang, Jian Peng, and Jianzhu Ma. Antigen-specific antibody design and optimization with diffusion-based generative models for protein structures. *Advances in Neural Information Processing Systems*, 35:9754–9767, 2022.

Appendix

Protein Representation Learning

Overview

Protein representation learning involves learning embeddings to convert raw protein data into latent space representations, extracting meaningful features and chemical attributes. More specifically, given a protein $x = [o_1, o_2, \dots, o_L]$, where each o_i represents an amino acid (sequence-based) or atom coordinate (structure-based), learn an embedding $z = [h_1, h_2, \dots, h_L]$, where each $h_i \in \mathbb{R}^d$ represents a d -dimensional token representation for amino acid o_i . This general framework can be extended to a multitude of tasks— for token property prediction tasks, additionally allocate a prediction $p(y_i|o_i)$ in the embedding, and for pairwise prediction tasks, allocate a prediction $p(y_{ij}|o_i, o_j)$. For overall protein property prediction, allocate predictions $p(y|x)$ or $p(y|x_1, x_2)$ for individual and protein-protein properties, respectively.

These embeddings can be seen as creating “richer” data spaces for various models to work on; whereas raw atom graphs and amino acid sequences are entirely arbitrary, these embeddings are aimed to capture various chemical traits and properties (i.e. two proteins with similar properties should be represented with similar embeddings, even if their raw forms are very different). Thus, representation learning models do not directly perform any tasks on their own, but instead are incorporated in other generative models to improve their ability to model these important chemical features.

Datasets

Note that a plethora of datasets exist for all various downstream tasks; we do not describe all such datasets. We focus on datasets used for pre-training in protein representation learning, described below. Note that UniRef, UniParc, and ProteinKG are typically used for sequence-based learning, and PDB and AlphaFoldDB are primarily used for structure-based learning. Pfam has been used in both types of models.

- **UniRef** [160] - A clustered version of the Unified Protein KnowledgeBase (UniProtKB), part of the central resource UniProt, which is a curated and labeled set of protein sequences and their functions
- **UniParc** [160] - A larger dataset of protein sequences, part of the central resource UniProt, which includes UniProtKB and adds proteins from a variety of other sources
- **ProteinKG** [38] - A dataset created by Zhang et al. (OntoProtein), aligning biological knowledge with protein sequences with knowledge graphs (KG), used for directly injecting biological knowledge in the representation learning process
- **PDB** [95] - *Protein Data Bank*, a central archive for all experimentally determined protein structures, widely used in almost all protein structure-related tasks.
- **AlphaFoldDB** [136] - *AlphaFold Protein Structure Database*, a large dataset created by using AlphaFold2 to predict structures from sequence datasets, such as UniProt and Swiss-Prot.
- **Pfam** [161] - A collection of protein families, used in multiple sequence alignments (MSA)

Tasks

Representation learning models do not directly address tasks on their own but rather supplement a wide range of tasks by refining a latent space. Thus, the protein

representation learning field in particular lacks uniformity in testing and training methods, making it hard to make generalized evaluations. Some methods like Tasks Assessing Protein Embeddings (TAPE) [162] and, more recently, Protein sEquence undERstanding (PEER) [163] seek to address this by compiling various testing metrics into a standardized benchmark for evaluating these language models. A few of the most prominent tasks include:

- **Contact Prediction** - Given two amino acid residues, predict the probability that they “contact”, or are within some 3D distance threshold. Measured using precision of top $L/5$ medium-range and long-range contacts (contact between sequentially distant amino acids) according to CASP standards [164].
- **Fold Classification** - Also known as remote homology prediction. Given an amino acid sequence, predict the corresponding fold class [165]. Used for finding structural similarities for distantly related inputs. Tested using the dataset proposed by Hou et al. [166], which comprises three versions of increasing difficulty: Family (test set in the same family as the training set), Superfamily (same superfamily as training) and Fold (same fold as training). Measured using accuracy.
- **Stability Prediction** - Given a protein, output a label $y \in \mathbb{R}$ representing the most extreme circumstances under which a protein maintains its fold above a concentration threshold. Measured using Spearman’s ρ .
- **PPI** - *Protein-Protein Interaction*, given two proteins, predict whether or not they interact (binary classification). Measured using accuracy.

Metrics

The following metrics are used to evaluate the above tasks:

- **Accuracy** - Ratio between correct classifications to total classifications.
- **Precision** - Accuracy within the set of selected elements; in contact prediction, this refers to the following: of the top $L/5$ contacts with the highest predicted probability, find the percentage of these which are ground-truth contacts. L refers to the length of a protein sequence.
- **Spearman’s ρ** - *Spearman’s rank correlation coefficient*, found by sorting the ground-truth and predicted output values into ranked order (so each protein has a true rank $y_i \in \mathbb{N}$ and predicted rank $x_i \in \mathbb{N}$) and computing:

$$\rho = 1 - \frac{6 \sum d_i^2}{n(n^2 - 1)},$$

where d_i refers to the numerical difference in ranks for each y_i, x_i , and n refers to the total number of elements in each set.

Models

As mentioned above, protein representation learning models can be divided into two broad categories: sequence-based and structure-based. This distinction simply refers to the type of input these models learn representations for; we begin by discussing sequence-based learning models. Both amino acid sequences and protein structures carry valuable information about a protein’s function and binding properties, and thus these two types of learning can be seen as complements to each other.

Unified Representation (UniRep) [167] used a multiplicative long-short-term memory recurrent neural network (mLSTM

Table 8. An overview of the most relevant sequence-based protein representation learning models. All metrics are self-reported unless otherwise noted; metrics reported by different papers may be incomparable due to different test settings. Note that OntoProtein and KeAP have two separate architectures for protein, and knowledge encoding respectively. [**] denotes the current SOTA.

Model	Type of Model	Dataset	Contact (\uparrow)	Fold Classification (\uparrow)			Stability (\uparrow)
				Family	Superfam.	Fold	
UniRep [167]	LSTM RNN	UniRef50	\	\	\	\	\
ProtBERT [116]	BERT	BFD100, UniRef100	0.556 [40]	0.528 [40]	0.192 [40]	0.170 [40]	0.651 [40]
ESM-1B [117]	Transformer	UniParc	0.458	0.978	0.601	0.268 [168]	0.695 [168]
MSA Trans. [169]	Transformer	26M MSAs	0.618 [40]	0.958 [40]	0.503 [40]	0.235 [40]	0.796 [40]
RSA** [40]	Transformer	Pfam	0.717	0.987	0.677	0.267	0.987
OntoProtein** [38]	ProtBERT, BERT/Trans.	ProteinKG*	0.40	0.96 [40]	\	0.24	0.75 [40]
KeAP** [39]	BERT, Transformer	ProteinKG	0.62	\	\	0.29	0.82
GearNET** [168]	Geo-EGNN	AlphaFoldDB	\	0.995	0.703	0.483	\
DeepFRI [170]	LSTM, GCNN	Pfam	\	0.732 [171]	0.206 [171]	0.153 [171]	\
IEConv [171]	CNN	PDB	\	0.997	0.806	0.503	\

RNN) to approach the task of representation learning. By iterating through each amino acid and comparing its prediction with the true amino acid type, adjusting its parameters at each step, UniRep gradually learns a better representation of the sequence. While the LSTM model has been proven inferior to newer transformer and natural language models, the basic concepts laid an important groundwork for future representation learning models.

ProtBERT [116] improved upon performance by applying a BERT model to amino acid sequences, treating each residue as a word. BERT stands for Bidirectional Encoder Representations from Transformers, which is a pre-trained language model for neural language processing. Several variations, such as RoBERTa and DeBERTa, improve upon BERT by enhancing parameters and attention mechanisms and are used in models discussed later. ESM-1B [117] trained a deep transformer with 33 layers and 650 million parameters, using the masked language modeling (MLM) objective for training. ESM-1b considered residue contexts across the entire sequence through its stacked attention layers, and its complexity and size allowed it to outperform other SOTA models on a wide range of tasks, as shown below. ESM-1b’s massive size also resulted in expensive training costs, however, and smaller research groups would had to find more unique approaches to compete with ESM-1b on representation learning.

Following ESM-1b’s breakthrough, a series of models applied the concept of direct knowledge injection. Previous models had simply treated these sequences as generic sequences of tokens, failing to take advantage of the vast biological knowledge in existence today. One avenue for knowledge injection comes from the analysis of Multiple Sequence Alignments (MSA), which groups proteins concerning their evolutionary families. Because inherent patterns appear as a result of the evolutionary process, analyzing MSAs can result in a richer understanding of protein sequences. MSA Transformer [169] was the first model to intersect a protein language model with MSA analysis, pretraining a transformer model on MSA input. While MSAs can provide large benefits, the alignment process is computationally costly. Retrieved Sequence Augmentation (RSA) [40] provides a solution to this, using a dense sequence retriever to directly augment input proteins with corresponding evolutionary information from the Pfam database. This allows RSA to incorporate similar information as traditional MSA methods, without the computationally costly MSA alignment process. OntoProtein [38] incorporates direct knowledge injection by pretraining on gene ontology (GO) knowledge graphs (KG). OntoProtein uses

the ProtBERT architecture for encoding protein sequences but introduces a second encoder for training on the GO input. To perform this hybrid encoding, Zhang et al. [38] create a new dataset, ProteinKG25, which aligns protein sequences with their respective GO annotations in text format. Knowledge-exploited Auto-encoder for Protein (KeAP) [39] extends upon this by exploring protein and annotated text on a more granular level; while OntoProtein models relationships over proteins and texts as a whole, KeAP uses a cross-attention mechanism to perform token-level exploration on individual amino acids and words.

Now, we discuss a few structure-based learning models. IEConv [171] incorporates both intrinsic distance (based on connectivity in a node-graph representation) and extrinsic distance (based on physical 3D distance) information in a convolutional neural network (CNN), using contrastive learning to pre-train. Additionally, IEConv uses protein-specific pooling methods, like reducing each amino acid to its alpha carbon, to reduce computational complexity and allow for more learned features per atom under memory constraints. DeepFRI [170] combines the idea of sequence representation learning with structural representation learning, incorporating both a pre-trained LSTM to learn sequence data and a GCN to learn from contact map input (matrix representing 3D distances between residues). GearNET [168] applies a GNN to a graph of residues, with three types of directed edges defined for sequential/physical distance and K-nearest neighbors. While previous models had only considered message-passing between residues, GearNET applied direct message-passing between edges in its variant model GearNET-Edge, which led to even further improved performance on various metrics. In addition, GearNET-IEConv added an intrinsic-extrinsic convolutional layer inspired by Hermosilla et al. [171] to improve performance, with GearNET-Edge-IEConv combining both of these features.

Antibody

Antibody Task Background

Antibodies are Y-shaped proteins used by the immune system to identify and neutralize foreign objects like bacteria and viruses. Each antibody contains two identical sets of chains, with each set containing one heavy chain and one light chain. The variable domains of these chains control binding specificity for various antigens, containing the binding surface, known as the paratope. The paratope binds with specificity to a target antigen at its respective binding region, known as the epitope. The paratope is typically located within six Complementarity-Determining Regions (CDRs) on the antibody: three from

Table 9. An overview of relevant antibody representation learning models. Due to the lack of standardization in benchmarking metrics, we note each model’s benchmarking findings.

Model	Type of Model	Dataset	AAR (% , \uparrow)	Additional Self-Benchmarking Notes
BERTTransformer [173]	BERT	OAS	\	Improved binding affinity prediction over generic CNN
AntiBERTy [120]	BERT	OAS	26.00 [121]	Reveals evolutionary trajectories for affinity maturation
AbLang [174]	RoBERTa	OAS	33.60 [121]	Clustering better represents distinction between B-cell type and other metrics (compared to ESM-1b)
PARA [121]	DeBERTa	OAS	34.20 [121]	Improved heavy/light chain matching (compared to AntiBERTy)
AntiBERTa [122]	RoBERTa	OAS	\	Clustering better represents distinction between B-cell type (compared to ProtBERT), improves paratope prediction

the light chain (CDR-L1, CDR-L2, CDR-L3) and three from the heavy chain (CDR-H1, CDR-H2, CDR-H3). The Complementary-Determining Region 3 (CDR-H3) is the most diverse in terms of amino acid sequence and length— due to its lack of constraints, it is often the most complex to produce, making its generation the primary focus for modern generative models.

The end goal of machine learning is to generate antibodies in silico. In approaching this goal, the typical pipeline often includes an amino acid sequence input, sequence representation learning, structure prediction, paratope-epitope prediction, antibody-antigen docking, CDR generation, and evaluation, typically in the form of affinity prediction. The final output is a generated antibody, either in the form of a 1D sequence, 3D structure, or both. Sometimes, a 3D structure is input directly, with the sequence being predicted from the structure. Machine learning methods have been applied to various fragments of the process, with some more recent models [172], [159], [158] handling both sequence and structure generation simultaneously, and others [159] even addressing the entire end-to-end process. Other subtasks like drug-applicable attribute prediction and affinity prediction have been explored using predictive AI models, but these tasks are not generative by nature and not be discussed in detail.

Antibody Representation Learning

Overview

This task is identical to the protein sequence representation learning, but language models in this field pretrain on antibody-specific data, in particular, outperforming general protein representation models on antibody-based tasks.

Datasets

All reported methods pre-train on the OAS dataset. In all methods, OAS was divided between heavy and light chains, with some [121, 174] also using Linclust to cluster the data. Leem *et. al* also includes pre-training on the general Pfam database for protein sequences, as a comparison to pre-training on the antibody-specific OAS dataset.

- **OAS** [175] - *Observed Antibody Space*, a compilation of over one billion raw antibody sequences.

Tasks

Given the variety of applications for representation learning, the benchmarks used for this task vary widely; some use Pearson correlation to measure affinity binding prediction [122], while others [121] use amino acid recovery (AAR) to measure accuracy in a CDR-H3 sequence prediction task. Some use a masked language modeling task (MLM) to measure the quality of BCR sequence representation [122], while others measure accuracy in paratope prediction [122, 120]. However, we do

not have a standardized benchmarking system as we did with protein representation learning, so we only report CDR-H3 sequence prediction in Table 9, which will be elaborated on more in the Antibody CDR Generation section (see page 25). Other evaluations are left as individual notes for each model.

Metrics

As noted above, we only report results on the CDR-H3 prediction task, which is measured with amino acid recovery (AAR), which represents the percentage of matching amino acids between ground truth and generated amino acid sequences.

Models

Li et al. [173] created the BERTTransformer model, serving as the first representation learning model aimed specifically at antibody learning. Li et al. find that pre-training on Pfam results in improved performance on affinity binding prediction when compared to pre-training on OAS, suggesting some merit to general protein datasets in pre-training for antibody representation learning. AntiBERTy [120] is a BERT-based model, and produces valuable embeddings used in structure prediction by IgFold [134]. AntiBERTa [122] and AbLang [174] both use the more optimized RoBERTa architecture, while the most recent model PARA [121] uses the current state-of-the-art DeBERTa architecture, and outperforms previous pre-trained models in AAR.

A comprehensive overview of representation learning models can be seen in Table 9. As representation learning serves as a general tool, rather than the optimization for a specific task, these methods all use a variety of self-chosen applications to measure performance. PARA tests amino acid recovery against AbLang and ‘ on the CDR-H3 prediction task, reporting improved accuracy. AntiBERTy and AntiBERTa report improved paratope prediction, while AbLang and AntiBERTa focus on improved clustering to distinguish between naive and memory B-Cells. AntiBERTa also explores clustering quality in terms of drug-applicable traits, such as origin, closest human V gene identity, and anti-drug antibody (ADA) response scores.

Antibody Structure Prediction

Overview

Antibody structure prediction extends general protein structure prediction methods, with the key difference lying in the reliance on multiple sequence alignment (MSA) of homologous proteins mapping evolutionary relationships between genetically related sequences. Because the relevant evolutionary histories for CDR-H3 loop sequences are lacking, MSAs in antibodies are not always available. This makes models like AlphaFold [130], designed for general protein structure prediction, highly inefficient and slow. Thus, antibody-specific structural

Model	Type of Model	Dataset	H3 RMSD (Å, ↓)	OCD (↓)	Generation Time (s, ↓)
IgFold** [134]	BERT, Graph	OAS, SAbDab	2.99	3.77 [134]	0.46 [134]
DeepAB [181]	LSTM, NN	OAS, SAbDab	3.28	3.6 [134]	1620.22 [135], 600 [134]
ABLooper [176]	EGNN	SAbDab, RAB	3.2	4.53 [134]	30-60 [134]
ImmuneBuilder [177]	AlphaFold - Multimer	SAbDab, RAB	2.81	4.9 [134]	5*
tFold-Ab** [135]	AlphaFold - Multimer	SAbDab	2.74	3.21 [134]	2.23* [135]
xTrimoABFold [182]	AlphaFold - Multimer	PDB	1.25	\	\

Table 10. An overview of the most relevant antibody structure prediction models. All benchmarking metrics are self-reported unless otherwise noted. Igfold and tFold-Ab use slightly different benchmarking methods, so their results may not be comparable. [*] denotes significant discrepancies which result from varying benchmarking methods. [**] denotes the current SOTA.

prediction methods seek to predict antibody structure without the need for an input MSA [134].

Datasets

Models in this field all train on the Structural Antibody Database (SAbDab), with the Rosetta Antibody Benchmark (RAB), used as a validation set in some cases [176, 177]. Note that “canonical conformations” do not exist for the highly variable H3 region due to high variability, which remains a challenge to structurally model.

- **SAbDab [178]** - *Structural Antibody Database*, a collection of all antibody structures in PDB [95]. Structures are annotated with antibody-specific structural data like canonical conformations for complementarity determining regions (CDR), orientation between the variable domains on the light and heavy chains, and the presence of constant domains in the structure.
- **RAB [179]** - *Rosetta Antibody Benchmark*, a hand-selected set of 60 antibody-antigen complexes, chosen to be as diverse in CDR lengths and clusters as possible.

Task

Given an antibody amino acid sequence (organized into heavy chain, light chain, and linker sequences), generate a set of 3D point coordinates for each amino acid residue.

Metrics

For benchmarking, models compare similarities between the predicted and ground truth structures through the following metrics:

- **RMSD** - *Root-mean-square deviation*, measures distances between ground truth and generated residue coordinates. Also used in protein structure prediction (see page 10)
- **OCD** [180] - *Oriental coordinate distance*, measures similarity between light-heavy orientational coordinates (LHOC) of ground truth and generated residues. LHOC is defined by Marze et al. [180], consisting of four metrics to measure orientation between light and heavy chains.

used root-mean-square deviation (RMSD) to measure the discrepancy between predicted and ground truth 3D structures, while some models [134], [181], [135] also used orientational coordinate distance (OCD) to measure the accuracy of predicted relative position between heavy and light chains in some cases.

Models

tFold-Ab [135], xTrimoABFold [182], and ABodyBuilder2 [177] all apply similar methods to AlphaFold, replacing the unnecessary MSA searching component. ABLooper [176] uses five EGNNs to each individually predict CDR structures, outputting the positional average of the five structures—this allows for the evaluation of confidence as the deviation

between these predicted structures. Some models do not predict structures directly: DeepH3 [183] uses a deep residual neural network to first predict structural restraints, using Rosetta to then output atomic structures. SimpleDH3 [184] adds ELMO embeddings to DeepH3, and DeepAb [181], the most recent version, adds interpretable attention layers to enhance output from the neural network.

Igfold [134] takes advantage of AntiBERTy’s [120] sequence embeddings to predict antibody structures using invariant point attention. While some other models, such as tFold-Ab [135], xTrimoABFold [182], and ABodyBuilder2 [177], demonstrate more accurate structures, IgFold produces structures at a superior speed, making it the established state-of-the-art model. Igfold’s downside is its reliance on PyRosetta to produce side-chain conformations, as the model Igfold itself only outputs backbone atoms. This adds significant time to the full process, as it takes around 0.46 seconds for Igfold to produce backbone atoms, but an additional 21.86 seconds, on average, for PyRosetta to convert these into full-atom structures [135]. By contrast, tFold-Ab [135] generates full-atom structures in less time than the Igfold + PyRosetta pipeline (2.23 seconds compared to 22.32 seconds).

Notably, in the training process, ImmuneBuilder and xTrimoABFold choose to include antibodies with identical sequences to expose models to antibodies with multiple conformations (identical sequences with different structures). On the other hand, DeepAB includes an entirely non-redundant set of sequences, seeking to expose its model only to unique items.

Table 10 presents detailed results for the performance of the discussed models. While IgFold does not have the absolute highest performance in terms of RMSD and OCD when compared to other methods, its speed makes it the state-of-the-art model. This speed advantage is contested only by tFold-Ab, which generates full-atom structures in less time than IgFold, as it circumvents IgFold’s reliance on computationally expensive Rosetta energy functions for side-chain prediction. Note that discrepancies in time results may result from varying benchmarking methods—time results from tFold-ab were reported on their own SAbDab-22H1-Ab/Nano dataset, while time results from IgFold were reported using their IgFold-Ab benchmark.

Antibody CDR Generation

Overview

CDR generation involves the generation of the variable regions of the antibody, directly determining binding affinity and making it the core of antibody generation. As mentioned above, the CDR-H3 region is the most variable, making it the most difficult region for models to generate and thus the primary region of focus.

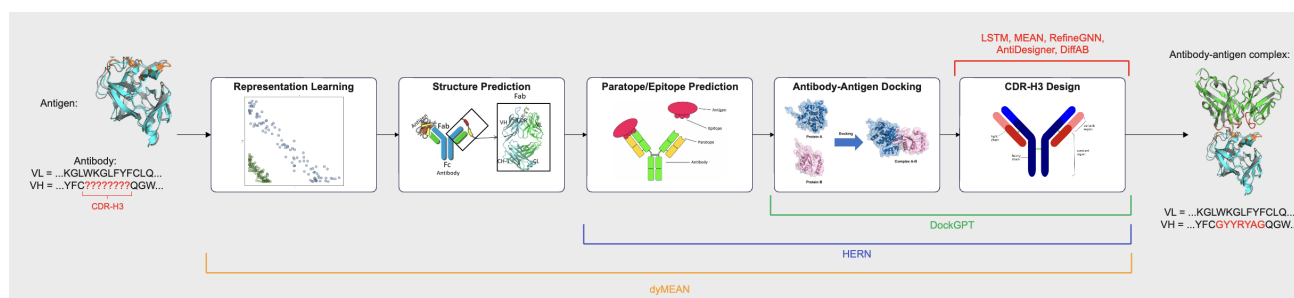


Fig. 5. A comprehensive overview of the antibody generation pipeline for CDR-H3 design. The inputs are a target antigen and antibody information (without CDR-H3), and the output is an antibody-antigen complex with a designed CDR-H3 sequence. Note that while most antibody CDR-H3 generation methods only generate the CDR-H3 region, needing a docked structure as input, some methods like DockGPT [185], HERN [186], and dyMEAN [159] perform multiple steps of the pipeline on their own. Images taken from [20, 23, 187, 188, 189].

Datasets

The primary datasets used in recent models are listed below. Note that SAbDab is the main dataset typically used for training, whereas RAbD and SKEMPI are specialized datasets used for testing specific downstream tasks.

- **SAbDab [178]** - *The Structural Antibody Database*, an annotated dataset of all antibody structures contained in PDB [95], used in structure prediction (see page 25)
- **RAB [179]** - *Rosetta Antibody Benchmark*, a hand-selected group of 60 diverse antibody-antigen complexes, also used in antibody structure prediction (see page 25).
- **SKEMPI [190]** - *Structural Database of Kinetics and Energetics of Mutant Protein Interactions*, a dataset of energy changes for mutations of protein-protein interactions.

Tasks

Three general tasks are used to benchmark models in this field:

- **Sequence and Structure Modeling** - Given an antibody structure, predict its corresponding sequence (or vice-versa). AAR is used to evaluate generated sequences, while RMSD is used to evaluate generated structures. Testing for this task is done on the SAbDab dataset.
- **CDR-H3 Generation** - Given a target antigen, generate the binding antibody CDR-H3 region. AAR is used to evaluate sequences, while RMSD and TM-Score are used to evaluate structures. Testing is done on the RAbD dataset.
- **Affinity Optimization** - Given an antibody-antigen pair, make changes to the CDR region to optimize its binding affinity with the target antigen. Performance is measured by $\Delta\Delta G$, and testing is done on SKEMPI v2.0.

Metrics

The following metrics are used to evaluate CDR generation models:

- **AAR** - *Amino acid recovery*, a comparison between ground truth and generated amino acid sequences, also measured in antibody representation learning (see 24).
- **RMSD** - *Root-mean-square deviation*, measures distances between ground truth and generated residue coordinates. Also used in protein structure prediction (see page 10)
- **TM-score** [128] - *Template Modeling Score*, a distance measurement capturing both local and global similarities, also used in protein structure prediction (see page 10).

- **$\Delta\Delta G$** - Change in binding energy after affinity optimization. Binding energy is predicted by the geometric network proposed by Shan et al. [191].

Models

While some approaches to the CDR generation problem have been sequence-based, such as the LSTM used by Akbar et al. [157], the field has seen movement towards structure-based design and even more recently, sequence-structure co-design, as this allows models to incorporate both 1D amino acid sequence information and 3D structure information in the generation process. RefineGNN [158] was the first to introduce structure/sequence co-design, representing both structural and sequential information in a graph and performing iterative refinement. A Multi-channel Equivariant Attention Network (MEAN) [172] improves efficiency by predicting all amino acids within a CDR region at once, allowing for fewer iterations than RefineGNN's prediction for each amino acid residue. AntiDesigner [192] implements a Protein Complex Invariant Embedding (PCIE) and dual Multi-Layer Perceptrons (MLPs) to design structures and sequences in a one-shot manner, removing the need for iterative refinement entirely. DiffAb [193] defines diffusion processes for both amino acid sequences and 3D backbone coordinates, serving as one of the first DDPMs in the field of antibody generation.

While the above models all show significant progress in the specific CDR generation task, these models still require the input of fully docked antibody-antigen structures; thus, in real-world applications where only sequence and/or structure data is available, these models must be paired with structure prediction and docking methods to operate. As a result, some methods simultaneously implement other parts of the antibody generation process in their model. The deep learning method DockGPT [185] includes an adaptation of their protein-protein docking method for antibody CDR-H3 docking and design. By adding an encoding feature to distinguish CDR residues during training and providing structures with missing CDR regions as input, DockGPT simultaneously docks and designs all CDR regions. HERN [186] uses hierarchical equivariant refinement to both generate and dock paratopes for target antigens. However, HERN requires a defined epitope region as input and needs to be combined with epitope prediction models to dock with antigens whose epitopes are not identified. Dynamic Multichannel Equivariant Graph Network (dyMEAN) [159] extends these ideas even further by creating the first end-to-end method, incorporating structure prediction, docking, and CDR generation in a singular model. To demonstrate its

Table 11. A summary of relevant CDR generation models. All benchmarking metrics are self-reported unless otherwise noted. dyMEAN and DiffAB use slightly different evaluation conditions, so their results may not be fully comparable. **[**]** denotes the current SOTA.

Model	Type of Model	Dataset	Modeling		CDR-H3 Design			Affinity
			AAR (% , \uparrow)	RMSD (\downarrow)	AAR (% , \uparrow)	TM-Score (\uparrow)	RMSD (\downarrow)	$\Delta\Delta G(\downarrow)$
LSTM [157]	LSTM	Self-made	15.69 [172]	\	22.36 [172]	\	\	-1.48 [172]
RefineGNN [158]	GNN	SAbDab	21.13 [172]	6 [172]	29.79 [172]	0.8308 [172]	7.55 [172]	-3.98 [172]
MEAN [172]	EGNN	SAbDab	36.38	2.21	36.77	0.9812	1.81	-5.33
AntiDesigner** [192]	MLP	SAbDab	37.37	1.97	40.94	0.985	1.55	-10.78
DiffAB [193]	Diffusion	SAbDab	26.78	3.597	35.31 [159]	0.9695 [159]	\	-2.17 [159]
DockGPT [185]	Transformer	SAbDab	\	\	\	\	1.88	\
HERN [186]	EGNN	SAbDab	\	\	34.1	\	\	\
dyMEAN** [159]	EGNN	SAbDab	\	\	43.65	0.9726	\	-7.31

improved performance, dyMEAN benchmarks against pipelines combining models for each subtask (Igfold \Rightarrow HDock \Rightarrow MEAN

to perform structure prediction, docking, and CDR generation, for example).